J. Fluid Mech. (2002), *vol.* 457, *pp.* 377–409.
DOI: 10.1017/S0022112002007796 Printed in the United Kingdom

A frictional Cosserat model for the slow shearing of granular materials

By L. SRINIVASA MOHAN†, K. KESAVA RAO AND PRABHU R. NOTT

Department of Chemical Engineering, Indian Institute of Science, Bangalore 560 012, India
e-mail: kesava@chemeng.iisc.ernet.in; prnott@chemeng.iisc.ernet.in

(Received 24 July 2001 and in revised form 10 October 2001)

A rigid-plastic Cosserat model for slow frictional flow of granular materials, proposed by us in an earlier paper, has been used to analyse plane and cylindrical Couette flow. In this model, the hydrodynamic fields of a classical continuum are supplemented by the couple stress and the intrinsic angular velocity fields. The balance of angular momentum, which is satisfied implicitly in a classical continuum, must be enforced in a Cosserat continuum. As a result, the stress tensor could be asymmetric, and the angular velocity of a material point may differ from half the local vorticity. An important consequence of treating the granular medium as a Cosserat continuum is that it incorporates a material length scale in the model, which is absent in frictional models based on a classical continuum. Further, the Cosserat model allows determination of the velocity fields uniquely in viscometric flows, in contrast to classical frictional models. Experiments on viscometric flows of dense, slowly deforming granular materials indicate that shear is confined to a narrow region, usually a few grain diameters thick, while the remaining material is largely undeformed. This feature is captured by the present model, and the velocity profile predicted for cylindrical Couette flow is in good agreement with reported data. When the walls of the Couette cell are smoother than the granular material, the model predicts that the shear layer thickness is independent of the Couette gap H when the latter is large compared to the grain diameter d_p. When the walls are of the same roughness as the granular material, the model predicts that the shear layer thickness varies as $(H/d_p)^{1/3}$ (in the limit $H/d_p \gg 1$) for plane shear under gravity and cylindrical Couette flow.

1. Introduction

The slow flow of densely packed granular materials is a subject of considerable importance, primarily due to the obvious commercial and technological implications resulting from a better understanding of granular flows. Granular materials are transported and processed in a variety of industrial operations, and furthering our knowledge of their rheology opens up the possibility of improving the design of these processes. The phrase 'slow flow' denotes the regime of where the density is high and the deformation rate low, so that momentum is mainly transferred during sustained contact between the grains, and the stress generated by grain collisions is insignificant. If we define the ratio of the stress arising from grain collisions to the total stress, $\mathscr{R} \equiv \rho_p d_p^2 \dot{\gamma}^2 / N$, where ρ_p and d_p are the density and mean diameter of the grains, $\dot{\gamma}$

† Present address: Fluent India Pvt. Ltd., South Koregaon park, Pune 411 001, India.

is the nominal shear rate and N is the total (normal or shear) stress, the slow flow regime corresponds to $\mathscr{R} \ll 1$. This is the case in many terrestrial flows, where gravity consolidates the medium to a state where sustained frictional contact occurs between the particles.

Experimental observations suggest that the drag force exerted by a granular medium when it flows slowly past a solid surface is not steady, but fluctuates in time (Budny 1979; Tüzün & Nedderman 1985; Munch-Andersen & Askegaard 1993; Nasuno *et al.* 1998; Albert *et al.* 2000). The oscillations diminish in magnitude as the flow velocity increases. In some cases, the amplitude of the oscillations is of the same order of magnitude as the mean value. This phenomenon is referred to as *stick-slip*. The frequency of the oscillations depends on the relative velocity between the granular material and the surface, and also on various other factors. In some of the studies cited above, the frequency was in the range of 0.05–100 Hz, and the relative velocity was in the range of $5\,\mu\mathrm{m\,s^{-1}}$–$10\,\mathrm{mm\,s^{-1}}$.

In this work we do not address the issue of stick-slip; rather we propose a hydrodynamic model for slow granular flows that can predict only the time-averaged values of the stress and velocity fields. It is assumed that the time-averaging is over a large number of stick-slip events. A prominent feature of the time-averaged stress in slow flow is its rate independence. For instance, Albert *et al.* (1999) found the drag force $\bar{F}$ on a vertical rod dipped into a rotating bed of glass beads to be independent of the velocity, for velocities in the range of 0.1–$1.5\,\mathrm{mm\,s^{-1}}$. Tardos, Khan & Schaeffer (1998) sheared granular materials in the annular gap of a vertical Couette cell, and measured the torque required to rotate the inner cylinder at a constant speed. For speeds in the range of 2.5–$50\,\mathrm{cm\,s^{-1}}$, which correspond to nominal shear rates in the range of 2–$40\,\mathrm{s^{-1}}$, $\bar{F}$ decreased very slightly as the shear rate increased; at higher shear rates, $\bar{F}$ increased with the shear rate.

As a first approximation in modelling the above experiments, we may assume that the drag force does not vary with the velocity. Within the framework of continuum mechanics, this is equivalent to the assumption that the constitutive equation relating the stress to the rate of deformation $\boldsymbol{D}$ is unaffected if all components of $\boldsymbol{D}$ are changed by a common factor. This is termed *rate-independent* behaviour. Rate-independent models for slow flow, which are usually based on concepts in metal plasticity and soil mechanics, have been used with some success for flow in hoppers and bunkers (Brennen & Pearce 1978; Cleaver & Nedderman 1993; Michalowski 1987).

However, these models fail for viscometric flows, in which the direction of variation of the velocity is orthogonal to the direction of flow. Experimental observations of viscometric flows, such as flow through vertical channels (Natarajan, Hunt & Taylor 1995; Nedderman & Laohakul 1980), or shear in a cylindrical Couette cell (Tardos *et al.* 1998) show large portions of the material not suffering sustained deformation, and shear occurring only in thin layers (Gudehus & Tejchman 1991; Nedderman & Laohakul 1980). Moreover, the thickness of the shear layer is influenced by the nature of the boundaries; it is less when the flowing medium is confined by smooth walls than in the case of rough walls (Nedderman & Laohakul 1980). In contrast, conventional plasticity-based models predict no shear layers (Mohan, Nott & Rao 1997; Tejchman & Wu 1993), with the entire region behaving like a rigid block and slipping relative to the walls.

Owing to the occurrence of narrow shear layers, the nominal shear rate differs significantly from the actual shear rate, making it difficult to interpret rheological data. A theory that predicts the extent of the locked, or 'plug', region and the velocity field within the shear layer would therefore be useful.

The inability of frictional models to determine the velocity field in viscometric flows has been attributed to the absence of a material length scale in their constitutive equations (Mühlhaus 1986, cited in Mühlhaus & Vardoulakis 1987). An attempt to correct this deficiency of the classical frictional models was recently made by Mohan, Nott & Rao (1999). They modelled the granular medium as a Cosserat continuum, which incorporates a material length scale in the constitutive equations. Cosserat plasticity models have previously been applied to problems in granular flow (Mühlhaus 1989; Mühlhaus & Vardoulakis 1987; Tejchman & Gudehus 1993; Tejchman & Wu 1993, 1994), but the models in these studies are posed in terms of strain increments as they only address unsteady flows, and no results are reported for steady flow.

In this work, we use the Cosserat model of Mohan *et al.* (1999) to examine steady shear between parallel plates and concentric cylinders. Unlike a classical continuum, a Cosserat continuum involves two additional field variables, namely the *intrinsic angular velocity* vector $\boldsymbol{\omega}$, and the *couple stress* tensor $\boldsymbol{M}$. The former represents the local rate of spin of material elements, and the latter represents the couple per unit area exerted by the medium. Hence the mass and linear momentum balances must be supplemented by the angular momentum balance relating the angular velocity vector, the stress tensor and the couple stress tensor. (In a classical continuum, the angular momentum balance is identically satisfied, and the angular velocity is equal to half the vorticity.) For steady, fully developed flow, spatial gradients of $\boldsymbol{M}$ cause the Cauchy stress $\boldsymbol{\sigma}$ to be asymmetric. To our knowledge, these effects have not been directly measured in the laboratory so far, and careful experiments in this direction would be of value. However, the consequences of our model are easily measurable even in simple viscometric flows, as we shall indicate later.

While there is no direct experimental evidence of stress asymmetry or deviation of the angular velocity from half of the vorticity, there is, however, sufficient motivation for treating a granular medium as a Cosserat continuum. In his analysis of the stress in a fluid composed of diatomic molecules, Dahler (1959) shows that an asymmetric Cauchy stress can result from the presence of non-central interaction forces between grains. Grain interactions in slow flows are dominated by frictional forces, which are inherently non-central. Jenkins, Cundall & Ishibashi (1989) constructed a micro-mechanical model for an assembly of identical spheres. They found that an asymmetric stress resulted when the distribution of contact normals was anisotropic. However, they secured symmetry of the stress tensor by suitably enforcing the rotation of particles. In his simulations of rapid shear of rough circular discs between parallel plates (the disks interacted through instantaneous collisions), Campbell (1993) observed that the stress tensor was asymmetric and that non-zero couple stresses existed near the walls. Therefore, a frictional Cosserat model may be an appropriate, and perhaps even the correct description, for slow granular flow.

2. Governing equations

As in a classical continuum, the mass and linear momentum balances are given by

$$\frac{\mathrm{D}\rho}{\mathrm{D}t} + \rho\nabla\cdot\boldsymbol{u} = 0, \tag{2.1}$$

$$\rho\frac{\mathrm{D}\boldsymbol{u}}{\mathrm{D}t} + \nabla\cdot\boldsymbol{\sigma} - \rho\boldsymbol{b} = 0. \tag{2.2}$$

Here $\mathrm{D}/\mathrm{D}t$ represents the material derivative, $\boldsymbol{u}$ the velocity, $\rho \equiv \rho_p v$ is the bulk density of the medium, ρ_p is the intrinsic density of the grains, v is the solids fraction,

$\boldsymbol{\sigma}$ the Cauchy stress tensor (defined in the compressive sense), and $\boldsymbol{b}$ the body force per unit mass. As discussed in the preceding section, for a Cosserat continuum these must be supplemented by the angular momentum balance (Jaunzemis 1967, p. 233) which takes the form

$$\rho \frac{\mathrm{D}(\mathscr{I} \cdot \boldsymbol{\omega})}{\mathrm{D}t} + \nabla \cdot \boldsymbol{M} - \boldsymbol{\varepsilon} : \boldsymbol{\sigma} - \rho \boldsymbol{\zeta} = 0. \tag{2.3}$$

Here $\mathscr{I}$ is the intrinsic inertia tensor, $\boldsymbol{\omega}$ is the intrinsic angular velocity, $\boldsymbol{M}$ is couple stress, $\boldsymbol{\varepsilon}$ is the alternating tensor and $\boldsymbol{\zeta}$ is the body couple. On a plane with unit normal $\boldsymbol{n}$, the couple per unit area transmitted to the side towards which $\boldsymbol{n}$ points (by the material on the other side) is $\boldsymbol{n} \cdot \boldsymbol{M}$. We follow the commonly used right-hand convention for the signs of $\boldsymbol{\omega}$ and $\boldsymbol{n} \cdot \boldsymbol{M}$. In general, the distribution of size, shape, and orientation of the particles is required to determine the inertia tensor $\mathscr{I}$. As the present work is confined to steady, fully developed flow, the term involving $\mathscr{I}$ in (2.3) vanishes.

Constitutive relations for $\boldsymbol{\sigma}$ and $\boldsymbol{M}$ for slow granular flow were proposed by Mühlhaus & Vardoulakis (1987) and Tejchman & Wu (1993) as extensions of the yield conditions and flow rules used in classical plasticity. Their relations are posed in terms of strains and strain increments, which they employed to study the temporal development of shear bands. Here we rewrite these relations in terms of the rate of deformation tensor, to render them in a form that is appropriate for sustained flow.

2.1. *Yield condition*

A commonly used model for a block sliding on a plane is that the shear force S_f is proportional to the normal force N_f, the constant of proportionality being the coefficient of friction μ. When the block does not slide, $S_f < \mu N_f$. The yield condition is a continuum analogue of this relation. For a classical continuum, it is of the form $F(\boldsymbol{\sigma}, \nu) = 0$, where F is a scalar function of the stress tensor $\boldsymbol{\sigma}$ and the solids fraction ν. As elastic effects are neglected, the material is rigid if $F < 0$. If $F = 0$, either plastic or irrecoverable deformation occurs, or the material is in a state of incipient yielding. The extended von Mises yield condition, used in some studies, has $F \equiv \tau(J_2) - Y(J_1, \nu)$ where J_1 is the first invariant (i.e. the trace) of $\boldsymbol{\sigma}$ and J_2 is the second invariant of the deviatoric stress tensor $\boldsymbol{\sigma}'$ (see below). To generalize this for a Cosserat continuum, we write τ as a function of J_2 and the couple stress $\boldsymbol{M}$, as described below.

Following Besdo (1974) (cited in Lippmann 1995), de Borst (1993) and Tejchman & Wu (1993), we take the yield condition to be given by

$$F \equiv \tau - Y = 0, \tag{2.4a}$$

where

$$\tau \equiv \left(a_1 \sigma'_{ij} \sigma'_{ij} + a_2 \sigma'_{ij} \sigma'_{ji} + \frac{1}{(L d_p)^2} M_{ij} M_{ij} \right)^{1/2}, \tag{2.4b}$$

$\sigma'_{ij} \equiv \sigma_{ij} - (1/3)\sigma_{kk}\delta_{ij}$ is the deviatoric stress, δ_{ij} is the Kronecker delta, a_1, a_2, and L are material constants, and d_p is the grain diameter. de Borst (1993) assumed that the yield function Y depends on the mean stress $\sigma \equiv \sigma_{kk}/3$ and a hardening parameter h. Here h is taken as the solids fraction ν, and hence $Y = Y(\sigma, \nu)$. The parameter $L d_p$ determines the characteristic material length scale, and is perhaps related to the length of force-chains (Howell, Behringer & Veje 1999).

Only two of the three parameters a_1, a_2 and L in (2.4*b*) are independent, because the third may be absorbed in the definition of $Y(\sigma, \nu)$ (see (2.4*a*)). Following Mühlhaus & Vardoulakis (1987) we set $a_1 + a_2 = 1/2$, without loss of generality. When $\boldsymbol{M}$

vanishes, the quantity τ in (2.4*b*) reduces $\sqrt{J_2}$, and hence the extended von Mises yield condition is recovered.

While it is desirable to determine the parameters independently, neither experiments nor micro-mechanical models are currently available to guide their choice. However, the condition $\tau^2 \geqslant 0$ imposes the bound $|a_2/a_1| \leqslant 1$, which follows from the result that the expression for τ^2 in (2.4*b*) is a quadratic form. We retain the value of 10 used by Mohan *et al.* (1999) for L, as it nicely fits experimental data for flow down vertical channels, and also their choice of $A \equiv a_2/a_1 = 1/3$. Nevertheless, we explore the sensitivity of the model predictions to these parameters in § 7.

The yield function $Y(\sigma, \nu)$ is usually written in the form $Y = Y_1(\alpha)\sigma_c(\nu)\sin\phi$, where $\alpha = \sigma/\sigma_c$, and $\sigma_c(\nu)$ is the mean stress at *critical state*, which is a state of deformation at constant density (see, for example, Jackson 1983). The parameter ϕ is a material constant called the angle of internal friction. For the problems considered in this paper, it is shown later that the material is everywhere at critical state, and hence $\alpha = 1$. The function $Y_1(\alpha)$ may then be set equal to 1 without loss of generality, and the yield condition reduces to

$$F = \tau - \sigma_c(\nu)\sin\phi = 0; \quad \sigma = \sigma_c(\nu) \tag{2.5}$$

at a critical state. We expect σ_c to vanish when the solids fraction is below that of loose random packing $\nu_{\min}$, when the grains are no longer in sustained contact, and to increase rapidly as ν approaches the solids fraction at dense random packing, $\nu_{\max}$.

However, we simplify the analysis in this work by assuming that the material is incompressible. Hence σ_c is treated as an primitive variable, and an explicit expression for $\sigma_c(\nu)$ is not required.

2.2. *Flow rule*

The flow rule relates the rate-of-deformation tensor to the stress tensor. A commonly used flow rule in classical frictional models is the plastic potential flow rule, which is expressed as

$$D_{ij} \equiv \frac{1}{2}\left(\frac{\partial v_i}{\partial x_j} + \frac{\partial v_j}{\partial x_i}\right) = \dot{\lambda}\frac{\partial G}{\partial \sigma_{ji}}. \tag{2.6}$$

Here D_{ij} is the rate-of-deformation tensor, $G(\boldsymbol{\sigma}, \nu)$ is scalar function called the *plastic potential*, and $\dot{\lambda}$ is a scalar factor which must be determined as a part of the solution. As detailed information on the plastic potential G is not usually available, we use the associated flow rule (Schofield & Wroth 1968, p. 43), for which

$$G \equiv F = \tau - Y. \tag{2.7}$$

This form for the flow rule, in conjunction with a yield condition defined by (2.4*a*, *b*), accounts for density changes accompanying deformation. Together, they constitute a rate-independent constitutive relation, which is a desirable feature for slow granular flows.

Tejchman & Wu (1993) used the approach of Mühlhaus (1989) to modify (2.6) for a Cosserat continuum, but posed it in terms of strain increments as they were addressing unsteady deformation. Because we are interested in sustained flow, we replace the plastic strain increments used by Tejchman & Wu (1993) by the appropriate deformation rates (Mühlhaus 1989), and thereby write the flow rule as

$$\boldsymbol{E} \equiv \nabla\boldsymbol{v} + \boldsymbol{\varepsilon}\cdot\boldsymbol{\omega} = \dot{\lambda}\frac{\partial F}{\partial \boldsymbol{\sigma}^t}, \quad \boldsymbol{H} \equiv \nabla\boldsymbol{\omega} = \dot{\lambda}\frac{\partial F}{\partial \boldsymbol{M}^t}. \tag{2.8a, b}$$

Here $\boldsymbol{\varepsilon}$ is the alternating tensor, and the superscript t indicates the transpose. Equations (2.8) may be written in Cartesian tensor notation as

$$E_{ij} = \frac{\partial v_i}{\partial x_j} + \varepsilon_{ijk}\omega_k = \dot{\lambda}\frac{\partial F}{\partial \sigma_{ji}}, \quad H_{ij} = \frac{\partial \omega_i}{\partial x_j} = \dot{\lambda}\frac{\partial F}{\partial M_{ji}}. \tag{2.9a,b}$$

We note here that E_{ij} is the sum of the rate-of-deformation tensor D_{ij} and an objective antisymmetric tensor representing the difference between the spin tensor and the particle spin $-\varepsilon_{ijk}\omega_k$. The quantities E_{ij} and H_{ij} are conjugate to the stress σ_{ji} and the couple stress M_{ji}, respectively, in the sense that the dissipation rate per unit volume by the contact forces and couples is given by $-(\sigma_{ji}E_{ij} + M_{ji}H_{ij})$ (Mühlhaus 1989).

If $\boldsymbol{M}$ vanishes and $\boldsymbol{\sigma}$ is symmetric, (2.9) reduces to

$$D_{ij} = \dot{\lambda}\frac{\partial F}{\partial \sigma_{ji}} \tag{2.10}$$

and

$$\varepsilon_{ijk}\omega_k = \frac{1}{2}\left(\frac{\partial v_j}{\partial x_i} - \frac{\partial v_i}{\partial x_j}\right), \quad \frac{\partial \omega_i}{\partial x_j} = 0. \tag{2.11}$$

Equation (2.10) is identical to the associated flow rule for the classical frictional model (defined by (2.6) with $G = F$). For steady flow, equation (2.11) implies that $\boldsymbol{\omega}$ is a constant, and is equal to half the vorticity. On the other hand, the vorticity need not be a constant in a classical frictional model. Thus, only some of the features of the latter are recovered in this special case.

As explained in § 10, the most important aspects of our results, i.e. the ability of the model to predict the velocity fields in viscometric flows and the dependence of the shear layer thickness on the properties of the material and the flow cell, are not specific to the particular forms of the constitutive relation chosen above, but have greater validity. The forms of the yield condition and flow rule we have chosen above serve to illustrate the importance of Cosserat effects in slow granular flows.

The application of the above Cosserat model to flow in vertical channels has been described in Mohan *et al.* (1999). Here we consider two other viscometric flows: (i) plane shear and (ii) cylindrical Couette flow. As rheological measurements are usually made in these geometries, it is useful to develop models for these cases.

3. Application to plane shear

Consider steady, fully developed flow between horizontal walls which are separated by a gap H (see figure 1). The upper wall moves in the positive x-direction with a constant speed V, the lower wall is stationary, and a constant compressive normal stress N is applied to the upper wall. (For the case of zero gravity, considered in § 5.1, the bottom wall is also subjected to a compressive normal stress of magnitude N.) Typically in an experiment, the initial gap, before the walls are set in motion, is fixed, at say H_0. Owing to dilation and compaction during shearing, this can change to a different value H once steady flow is established.

The velocity fields are of the form

$$\left.\begin{array}{lll} v_x = v_x(y), & v_y = 0, & v_z = 0, \\ \omega_x = 0, & \omega_y = 0, & \omega_z = \omega_z(y), \end{array}\right\} \tag{3.1}$$

and all the stresses are assumed to depend only on the y-coordinate. Equations (3.1)

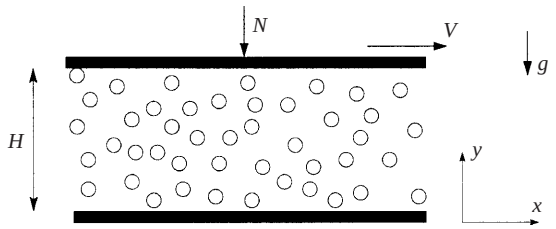

FIGURE 1. Plane shear between parallel walls. The lower wall is stationary and the upper wall moves at a constant speed V. A constant normal stress N is applied on the upper wall. The angles of wall friction of the lower and upper walls are δ_L and δ, respectively.

and (2.1) imply that $\mathrm{D}\rho/\mathrm{D}t = 0$. Hence the material is at a critical state, and the yield condition is given by (2.5).

The mass balance (2.1) is identically satisfied, and the x- and y-components of the linear momentum balance (2.2) reduce to

$$\frac{\mathrm{d}\sigma_{yx}}{\mathrm{d}y} = 0, \quad \frac{\mathrm{d}\sigma_{yy}}{\mathrm{d}y} = -\rho g. \tag{3.2a,b}$$

As there is no externally imposed body couple, the z-component of the angular momentum balance reduces to

$$\frac{\mathrm{d}M_{yz}}{\mathrm{d}y} + \sigma_{xy} - \sigma_{yx} = 0. \tag{3.3}$$

The diagonal components of E_{ij} are zero, and hence the flow rule (2.9) implies that

$$0 = \frac{\dot{\lambda}}{6\tau}(2\sigma'_{xx} - \sigma'_{yy} - \sigma'_{zz}), \tag{3.4a}$$

$$0 = \frac{\dot{\lambda}}{6\tau}(2\sigma'_{yy} - \sigma'_{xx} - \sigma'_{zz}), \tag{3.4b}$$

$$0 = \frac{\dot{\lambda}}{6\tau}(2\sigma'_{zz} - \sigma'_{xx} - \sigma'_{yy}). \tag{3.4c}$$

As $\sigma'_{ij} = \sigma_{ij} - \sigma\delta_{ij}$, we have $\sigma'_{xx} + \sigma'_{yy} + \sigma'_{zz} = 0$. Hence, (3.4) imply equality of the normal stresses,

$$\sigma_{xx} = \sigma_{yy} = \sigma_{zz} = \sigma = \sigma_c(v). \tag{3.5}$$

From (3.1) and (2.9), we have

$$E_{xz} = E_{zx} = E_{yz} = E_{zy} = 0,$$

which imply that all the shear stresses except σ_{xy} and σ_{yx} vanish. Similarly, all the couple stresses except M_{yz} vanish. Hence the yield condition (2.4a) reduces to

$$\tau^2 = a_1(\sigma_{xy}^2 + \sigma_{yx}^2) + 2a_2\sigma_{xy}\sigma_{yx} + \frac{M_{yz}^2}{(L\,d_p)^2} = (\sigma_c \sin\phi)^2. \tag{3.6}$$

The remaining equations of the flow rule (2.9) are

$$E_{xy} = \frac{\mathrm{d}v_x}{\mathrm{d}y} + \omega_z = \frac{\dot{\lambda}}{\tau}(a_1\sigma_{yx} + a_2\sigma_{xy}), \tag{3.7}$$

$$E_{yx} = -\omega_z = \frac{\dot{\lambda}}{\tau}(a_1\sigma_{xy} + a_2\sigma_{yx}), \tag{3.8}$$

$$H_{zy} = \frac{\mathrm{d}\omega_z}{\mathrm{d}y} = \frac{\dot{\lambda}}{\tau}\frac{M_{yz}}{(Ld_p)^2}. \tag{3.9}$$

Eliminating $\dot{\lambda}$ from (3.7)–(3.9), we obtain

$$\frac{\mathrm{d}v_x}{\mathrm{d}y} = -\frac{(A+1)(\sigma_{xy}+\sigma_{yx})\omega_z}{\sigma_{xy}+A\sigma_{yx}}, \tag{3.10}$$

$$\frac{\mathrm{d}\omega_z}{\mathrm{d}y} = -\frac{\omega_z}{(Ld_p)^2}\frac{2(A+1)m}{(\sigma_{xy}+A\sigma_{yx})}. \tag{3.11}$$

Equations (3.2), (3.3), (3.6), and (3.10)–(3.11) constitute the governing equations for plane shear. They may be cast in dimensionless form by introducing the dimensionless variables

$$\xi = \frac{y}{H}, \quad u = \frac{v_x}{V}, \quad \bar{\sigma}_{ij} = \frac{\sigma_{ij}}{N}, \quad m = \frac{1}{L\sqrt{2(A+1)}}\frac{M_{yz}}{(Nd_p)}, \quad \omega = \frac{\omega_z H}{V}. \tag{3.12}$$

The governing equations now take the form

$$\frac{\mathrm{d}\bar{\sigma}_{yx}}{\mathrm{d}\xi} = 0, \tag{3.13}$$

$$\frac{\mathrm{d}\bar{\sigma}_{yy}}{\mathrm{d}\xi} + Bv = 0, \tag{3.14}$$

$$\varepsilon\alpha\frac{\mathrm{d}m}{\mathrm{d}\xi} + \frac{1}{2(A+1)}(\bar{\sigma}_{xy}-\bar{\sigma}_{yx}) = 0, \tag{3.15}$$

$$(\bar{\sigma}_{xy}^2+\bar{\sigma}_{yx}^2) + 2A\bar{\sigma}_{xy}\bar{\sigma}_{yx} + 4(A+1)^2m^2 - 2(A+1)(\bar{\sigma}_c\sin\phi)^2 = 0, \tag{3.16}$$

$$\frac{\mathrm{d}u}{\mathrm{d}\xi} + \frac{(A+1)(\bar{\sigma}_{xy}+\bar{\sigma}_{yx})\omega}{\bar{\sigma}_{xy}+A\bar{\sigma}_{yx}} = 0, \tag{3.17}$$

$$\varepsilon\alpha\frac{\mathrm{d}\omega}{\mathrm{d}\xi} + \frac{2(A+1)m\omega}{(\bar{\sigma}_{xy}+A\bar{\sigma}_{yx})} = 0. \tag{3.18}$$

where $\varepsilon \equiv d_p/H$, $B \equiv \rho_p g H/N$ is ratio of the gravitational head at the base to the applied normal stress on the top plate, and $\alpha \equiv L/\sqrt{2(A+1)}$.

The yield condition (3.16) may be solved for $\bar{\sigma}_{xy}$ to obtain

$$\bar{\sigma}_{xy} = -A\bar{\sigma}_{yx} \pm \sqrt{(A^2-1)\bar{\sigma}_{yx}^2 + 2(A+1)\bar{\sigma}_c^2\sin^2\phi - 4(A+1)^2m^2}, \tag{3.19}$$

where $\bar{\sigma}_c = \sigma_c/N$.

4. Boundary conditions

Equations (3.13)–(3.19) require five boundary conditions. We first consider boundary conditions for the linear and angular momentum balances (3.13)–(3.15). The first is the specification of the normal stress N acting on the upper wall, i.e.

$$\bar{\sigma}_{yy}(1) = 1. \tag{4.1}$$

If the material slips relative to a wall, we use the usual friction boundary condition (Brennen & Pearce 1978; Nedderman 1992, p. 41),

$$-\bar{\sigma}_{yx}/\bar{\sigma}_{yy} = \tan\delta, \tag{4.2}$$

where δ, the angle of wall friction, is a property of the wall and the granular material. This is an approximate time-averaged boundary condition and is not expected to capture rapid events such as stick-slip. For the special case of shear in the absence of gravity between identical walls, (4.2) applies on both walls, which is equivalent to specifying (4.2) at one wall and $m(\xi = 1/2) = 0$, as elaborated in § 5.1. We therefore have the requisite number of boundary conditions for (3.13)–(3.15).

As discussed in Kaza (1982) and Nedderman (1992, p. 161), the classical frictional model suggests that $\tan\delta \leqslant \sin\phi$. A 'fully rough' wall is defined as one for which the angle of wall friction satisfies

$$\tan\delta = \sin\phi. \tag{4.3}$$

Physically we may try to realize this by coating the wall with a monolayer of the granular material. In some experiments involving walls coated with sand, polystyrene beads and glass beads, the measured values of δ were found to be within 1° of the values predicted by (4.3) (Kaza 1982). However, (4.3) should not be taken too seriously, as it rests on assumptions which are difficult to verify. Moreover, it is well known that grains do not pack as densely near a solid boundary as in the bulk; hence it is reasonable to suppose that a fully rough wall is an idealization that is difficult to achieve practically.

When the material does not slip relative to a wall (as is the case in most of the problems considered in § 5), friction is not fully mobilized and an alternative to (4.2) must be specified. One choice is to specify the value of m ($= m_w$) at the wall. In this work, we use the condition

$$\bar{\sigma}_{xy} = \bar{\sigma}_{yx} \tag{4.4}$$

at a wall where the material does not slip relative to it. This is equivalent to specifying m_w, as it can then be expressed in terms of σ_{yx} using (4.4) and the yield condition (3.16). Equation (4.4) was motivated by an expectation that Cosserat effects such as the stress asymmetry would vanish outside the shear layer. However, the results presented later do not support this conjecture. Fortunately, the velocity profile is relatively insensitive to the value of m_w, as discussed in § 5.

We now consider boundary conditions for the flow rule (3.17)–(3.18). If the material slips relative to a boundary, we assume as in our earlier work (Mohan *et al.* 1999) that

$$\boldsymbol{v} - \boldsymbol{v}_w = -K d_p \boldsymbol{n} \times \boldsymbol{\omega}, \tag{4.5}$$

where K is a dimensionless constant which reflects the roughness of the wall, $\boldsymbol{n}$ is the unit normal at the wall (pointing into the granular material) and $\boldsymbol{v}_w$ is the linear velocity of the wall. This boundary condition relates the angular velocity of the material adjacent to the wall to the slip velocity. It was introduced by Tejchman & Gudehus (1993) and Tejchman & Wu (1993), who formulated it in terms of displacement and rotation. Here we use an equivalent form in terms of velocity and angular velocity.

An explanation of this condition was provided by Mohan *et al.* (1999), which we repeat here for the sake of completeness. If we consider a single spherical particle moving past a stationary wall, the linear velocity $\boldsymbol{v}'$ of its centre of mass and the angular velocity $\boldsymbol{\omega}'$ about an axis passing through the centre of mass are related by $\boldsymbol{v}' = (d_p/2)\boldsymbol{n} \times \boldsymbol{\omega}'$ if the particle rolls without slipping. Conversely, if the particle slides without rolling, $\boldsymbol{\omega}' = 0$ but $\boldsymbol{v}'$ is arbitrary. For the boundary condition (4.5), these limits correspond to $K \to 1/2$ and $K \to \infty$, respectively. If the particles are rough or angular, rolling and slipping may be altogether absent, reducing the lower limit of

K to zero. In a continuum description, we expect that K will decrease as the wall roughness increases. It is reasonable to expect that K and the angle of wall friction δ are related, as they both characterize the roughness of the wall. However, as data bearing on this are lacking, both K and δ will be treated as independent parameters.

For the present problem, (4.5) may be written in dimensionless form as

$$u(1) = 1 + \varepsilon K \omega(1) \tag{4.6}$$

if (4.2) holds at the upper wall, and

$$u(0) = -\varepsilon K \omega(0) \tag{4.7}$$

if (4.2) holds at the lower wall.

If the material does not slip relative to the upper wall, we have

$$u(1) = 1. \tag{4.8}$$

Similarly, if the material does not slip relative to the lower wall, we have

$$u(0) = 0. \tag{4.9}$$

5. Results for plane shear

We start by considering the case of zero gravity, for which the parameter B in (3.14) is set to zero. We then consider finite gravity, for which B determines the gravitational overburden at the base in comparison with the applied normal load.

5.1. *Shear in the absence of gravity*

We first consider the case where the two walls are identical, i.e. $\delta_L = \delta$, where δ_L and δ are the angles of wall friction of the lower and upper walls, respectively. The domain is symmetric about the mid-plane $\xi = 1/2$, and (3.13)–(3.18) admit a solution wherein the stresses are symmetric and m is antisymmetric about $\xi = 1/2$. Similarly $u - 1/2$ is antisymmetric while the angular velocity ω is symmetric about $\xi = 1/2$. It then suffices to solve the problem in the half-domain $1/2 \leqslant \xi \leqslant 1$, with boundary conditions

$$m(1/2) = 0, \quad u(1/2) = 1/2, \tag{5.1a,b}$$

and (4.1), (4.2) (at $\xi = 1$), and (4.6). The momentum balances (3.13) and (3.14) and the boundary conditions (4.1) and (4.2) imply that

$$\bar{\sigma}_{yy} = 1, \quad \bar{\sigma}_{yx} = -\tan\delta. \tag{5.2}$$

Hence (3.5) implies that the solids fraction v is also a constant, and its value is given by $\bar{\sigma}_c(v) = 1$. Substituting for $\bar{\sigma}_{xy}$ from (3.19) into the angular momentum balance (3.15) yields the following equation for the couple stress:

$$\alpha\varepsilon \frac{\mathrm{d}m}{\mathrm{d}\xi} = -a \mp \sqrt{b^2 - m^2}, \tag{5.3}$$

where

$$a = \frac{\tan\delta}{2}, \quad b = \left(a^2 + \frac{1}{2(A+1)} (\sin^2\phi - \tan^2\delta) \right)^{1/2}. \tag{5.4}$$

This must be solved for m in the region $1/2 \leqslant \xi \leqslant 1$ with boundary condition (5.1). The shear stress $\bar{\sigma}_{xy}$ then follows from (3.19).

Let us consider the choice of sign on the right-hand side of (5.3). If the negative

sign is used in front of the square root, $\mathrm{d}m/\mathrm{d}\xi < 0$. Equation (5.1) implies that $|m|$ increases as ξ increases from 1/2. Therefore, for small enough values of ε, $m = -b$ at some value of $\xi = \xi_r < 1$, and hence a real-valued solution cannot be constructed for $\xi > \xi_r$. We therefore choose the positive sign in front of the square root. This leads to an acceptable solution because, though $\mathrm{d}m/\mathrm{d}\xi \geqslant 0$, the structure of (5.3) ensures that $|m| \leqslant \sqrt{b^2 - a^2}$. This choice of roots is used throughout the paper. It corresponds to the use of the negative sign in front of the square root in (3.19).

The differential equation (5.3) may be integrated by making the substitution $m = b \sin\psi$, to obtain

$$\frac{\xi - 1/2}{\alpha\varepsilon} = \psi + \frac{a}{\sqrt{b^2 - a^2}} \ln\left(\frac{c + \tan(\psi/2)}{c - \tan(\psi/2)}\right) \tag{5.5}$$

with $c = \sqrt{b - a}/\sqrt{b + a}$. The velocity fields must be determined by integrating (3.17) and (3.18) numerically subject to the boundary conditions (4.6) and (5.1*b*).

Before discussing results for arbitrary values of the angle of wall friction δ, it is instructive to consider the special case of a fully rough wall, defined by (4.3), for which $b = a$. In this case, (5.3) and (5.1*a*) imply that m and all its derivatives with respect to ξ vanish at $\xi = 1/2$, resulting in $m(\xi) = 0$. It then follows that

$$\bar{\sigma}_{xy} = \bar{\sigma}_{yx} = -\tan\delta, \tag{5.6a}$$

$$\omega = \omega_1 \text{ (constant)}, \tag{5.6b}$$

$$u = 1/2 - 2\omega_1(\xi - 1/2). \tag{5.6c}$$

Using the boundary condition (4.6), we obtain

$$\omega_1 = -1/(2 + 2\varepsilon K). \tag{5.6d}$$

As expected from the direction of motion of the upper plate (figure 1), ω_1 is negative, implying that the particles rotate about the z-axis in the clockwise direction. If the gap width is large compared to the particle diameter, $\varepsilon \to 0$ and therefore $u(1) \to 1$. Thus the velocity slip at the walls vanishes when thick layers are sheared.

Thus the couple stress vanishes, the stress tensor is symmetric, and the angular velocity is equal to half the vorticity, all of which are features of a classical continuum. However, the classical frictional model does not lead to a unique velocity profile, unlike the Cosserat model. As noted earlier, this is because the two models are not identical for this special case.

For $\tan\delta < \sin\phi$, rather than determining m by solving (5.5) and then the velocity fields by integrating (3.17)–(3.18), all the fields are obtained by integrating (3.15)–(3.18), after substituting for $\bar{\sigma}_{xy}$ from (3.19). This is done because such a numerical solution procedure is required for plane shear under gravity and cylindrical Couette flow, as analytical solutions could not be constructed for these problems. The system of equations were solved numerically using the LSODA routine (Petzold 1983) from the ODEPACK library in NETLIB. Our numerical procedure was verified by favourable comparison with the analytical solution given by (5.5), and the asymptotic solutions in the Appendix (see figures 4 and 7).

Figure 2 shows the velocity and stress profiles for different values of the angle of wall friction δ. The velocity profile is linear for the case of fully rough walls ($\tan\delta = \sin\phi$), and becomes curved as the difference between $\sin\phi$ and $\tan\delta$ increases. Correspondingly, the thickness of the shearing layer decreases. Panels (*b*) and

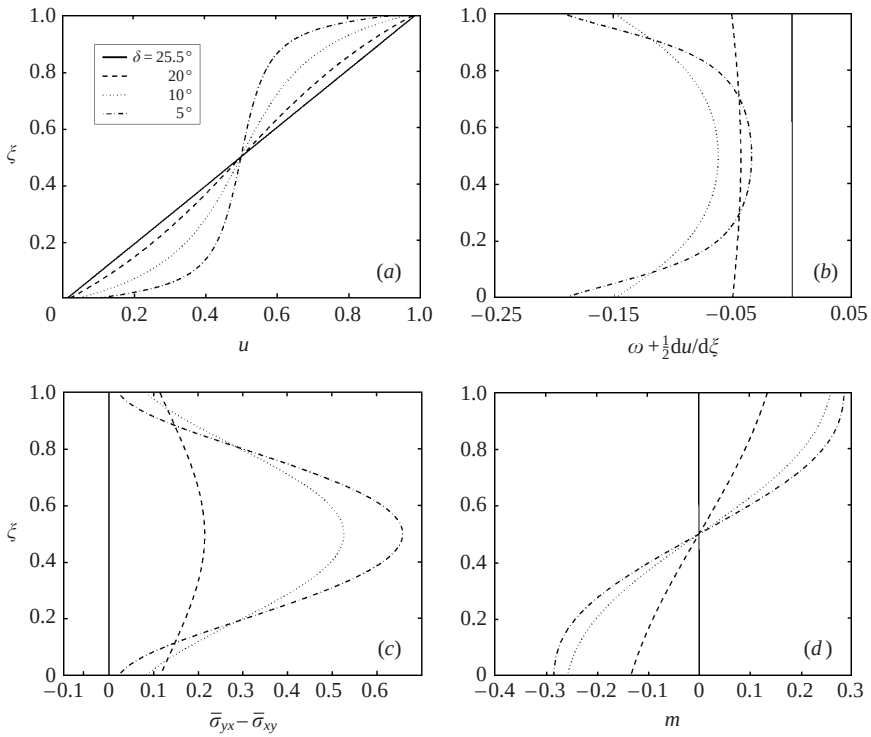

FIGURE 2. Velocity and stress profiles from the Cosserat model for shear between identical walls in the absence of gravity, for different values of the angle of wall friction δ: (b) shows the difference between ω and half the vorticity ($-(1/2)\,\mathrm{d}u/\mathrm{d}\xi$), and ($c$) shows the asymmetry in the shear stress. The material shears uniformly when the walls are fully rough (solid line). The thickness of the shear layer decreases as the difference between $\sin\phi$ and $\tan\delta$ increases. Parameter values are: $\phi = 28.5°$, $\varepsilon = 0.04$, $L = 10$, $A = 1/3$ and $K = 0.5$.

(c) illustrate the deviation of ω from half the vorticity and the stress asymmetry, respectively. The choice of signs in (3.19) forces $\bar{\sigma}_{yx} - \bar{\sigma}_{xy}$ to be non-negative.

When the angle of friction of the lower wall (δ_L) differs from that of the upper wall (δ), the solution is no longer symmetric about $\xi = 1/2$. We assume without loss of generality that $\delta_L > \delta$. If the friction boundary condition (4.2) is satisfied at the upper wall, $-\bar{\sigma}_{yx}/\bar{\sigma}_{yy} = \tan\delta < \tan\delta_L$. Hence (4.2) is not satisfied at the lower wall. Conversely, if (4.2) is satisfied at the lower wall, $-\bar{\sigma}_{yx}/\bar{\sigma}_{yy} = \tan\delta_L > \tan\delta$ at the upper wall. As this is not permissible within the present framework, (4.2) is used at the upper wall, along with the velocity boundary condition (4.6). At the lower wall we use boundary condition (4.4) for the couple stress, and the no-slip condition (4.9).

Equations (3.15) and (4.4) imply that $\mathrm{d}m/\mathrm{d}\xi = 0$ at $\xi = 0$. It then follows from (5.3) that all higher derivatives of m vanish at $\xi = 0$. Hence, the couple stress is constant and the shear stresses are equal,

$$m = m_0 = (b^2 - a^2)^{1/2}, \tag{5.7a}$$

$$\bar{\sigma}_{xy} = \bar{\sigma}_{yx} = -\tan\delta. \tag{5.7b}$$

Substitution of these in (3.17) yields

$$\frac{\mathrm{d}u}{\mathrm{d}\xi} = -2\omega.$$

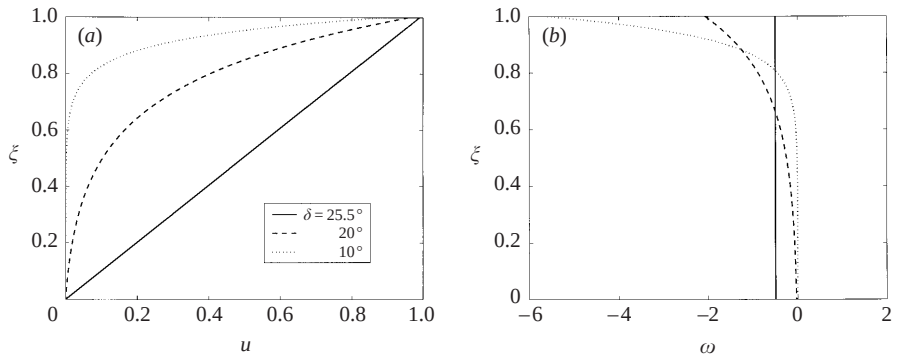

FIGURE 3. The velocity and angular velocity profiles for plane shear in the absence of gravity when the lower wall is rougher than the upper wall, i.e. $\delta_L > \delta$. For this problem, the stress is symmetric, the couple stress is constant (see (5.7)), and the angular velocity is equal to half the vorticity. The material shears uniformly when the upper wall is fully rough (solid line). Other parameters are given in the caption of figure 2.

Thus, the stress tensor is symmetric and the angular velocity is equal to half the vorticity, as in a classical continuum. However, the couple stress is finite and the velocity field is uniquely determined, in contrast to the predictions of a classical frictional model. The velocity fields are readily obtained by integrating (3.17)–(3.18), resulting in

$$\omega = \omega_1 \exp(-k(1-\xi)/\varepsilon), \tag{5.8a}$$

$$u = \frac{-2\omega_1\varepsilon}{k}(\exp(-k(1-\xi)/\varepsilon) - \exp(-k/\varepsilon)), \tag{5.8b}$$

where

$$\omega_1 = -\varepsilon^{-1}(2/k + K - 2e^{-k/\varepsilon}/k)^{-1} \tag{5.8c}$$

is the angular velocity at the upper wall and

$$k = m_0/(\alpha a). \tag{5.8d}$$

We see from equation (5.8*b*) that the shear layer thickness increases with the roughness of the upper wall. The velocity profile becomes progressively linear as $\tan\delta \to \sin\phi$ (or $k \to 0$). However, the velocity profile in this limit still differs from the uniformly shearing solution given in (5.6*c*), owing to the difference in velocity boundary conditions at the lower wall in the two cases. Profiles of the velocity and angular velocity (which equals half the vorticity) fields are shown in figure 3 for three values of δ. The increasing localization of shear near the upper wall as δ decreases is apparent. In this case, the velocity slip at the upper wall is non-zero in the limit $\varepsilon \to 0$. This is in contrast to the case of shear between fully rough walls, where the velocity slip vanishes in this limit.

When the Couette gap is large compared to the grain size, i.e. $\varepsilon \ll 1$, an approximate solution may be obtained by an asymptotic analysis, described in the Appendix. For shear between identical walls, the couple stress is constant and the Cauchy stress is symmetric, i.e.

$$m = m_0 = (b^2 - a^2)^{1/2}, \quad \bar{\sigma}_{xy} = \bar{\sigma}_{yx} = -\tan\delta, \tag{5.9a,b}$$

except in a boundary layer of thickness $\sim O(\varepsilon)$ near $\xi = 1/2$. In the boundary layer, m decreases from m_0 to zero at $\xi = 1/2$, but this variation has no effect on the velocity fields (see the Appendix, § A.1). There is no boundary layer when one of the walls is

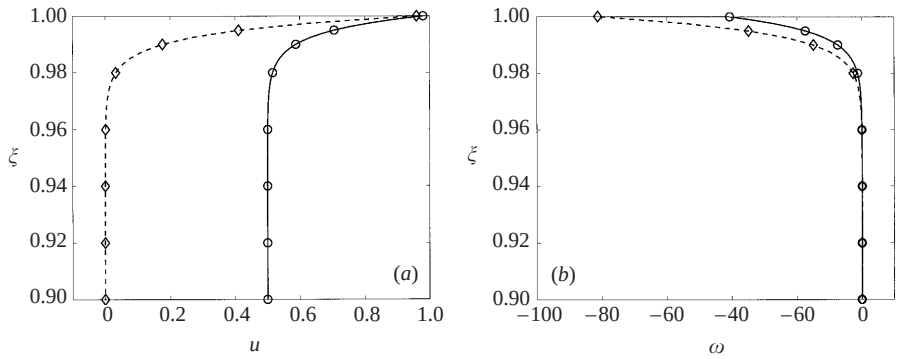

FIGURE 4. Comparison of the asymptotic solutions (for small ε) for (a) the linear velocity and (b) the angular velocity fields with their respective numerical solutions, for plane shear in the absence of gravity. The solid line and circles represent numerical and asymptotic solutions, respectively, for shear between identical walls. The dashed line and diamonds represent numerical and asymptotic solutions, respectively, for the case of a rougher lower wall. Parameter values are: $\phi = 28.5^\circ$, $\delta = 20^\circ$, $\varepsilon = 10^{-3}$, $L = 10$, $A = 1/3$ and $K = 0.5$.

rougher. The leading-order velocity fields for the two cases, given in (A 3) and (A 4), may be combined and written as

$$\omega = \frac{-(1-u_0)}{\varepsilon(K+2/k)} \exp(-k(1-\xi)/\varepsilon), \tag{5.9c}$$

$$u - u_0 = \frac{(1-u_0)2/k}{(K+2/k)} \exp(-k(1-\xi)/\varepsilon). \tag{5.9d}$$

Here u_0 is the reference velocity, equal to $1/2$ (the velocity at the symmetry axis) for shear between identical walls, and zero (the velocity of the lower wall) for a rougher lower wall. The rapid decay of ω and u with distance from the wall is apparent. Equation (5.9) is not valid when the walls are fully rough, as we have assumed in its derivation that $k \gg \varepsilon$ (see § A.1); as stated earlier, all Cosserat effects vanish and the material shears uniformly in the gap when the walls are fully rough. The asymptotic solution for the velocity fields (5.9c, d) agrees well with the numerical solution for shear between identical walls and for the case of a rougher lower wall (figure 4). The dependence of the shear layer thickness on ε is discussed in § 8.

As discussed in § 4, we do not have a rigorous basis for the boundary condition (4.4) for the case of a rougher lower wall. A study of the sensitivity of the model predictions to varying the boundary condition is therefore in order. The imposition of any condition for the angular momentum at the lower wall is equivalent to specifying the value of the couple stress there. In particular, the boundary condition (4.4) is equivalent to $m(0) = m_0$, where m_0 is defined by (5.7a). For the shear stress $\bar{\sigma}_{xy}$ to be real, (5.3) implies that the maximum value $m(0)$ can take is b, defined in (5.4); for ω and the velocity gradient to increase in magnitude with distance from the lower wall (as is physically reasonable) the flow rule (3.17)–(3.18) dictates that the minimum value $m(0)$ can take is zero. As shown in figure 5, the value of $m(0)$ has a negligible effect on the velocity profile. The reason for this result is that the couple stress approaches a common asymptote as $\xi \to 1$ for all values of $m(0)$ (see also § A.2). As the velocity and angular velocity fields decay exponentially with distance from the upper wall, with a decay length set by the couple stress near the upper wall,

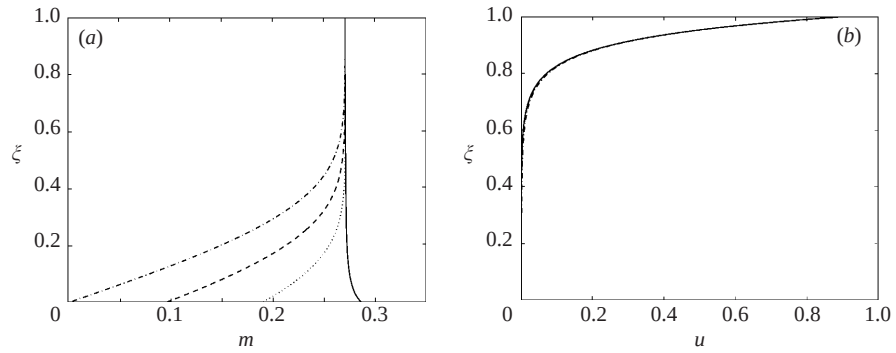

FIGURE 5. Effect of $m(0)$, the boundary condition for the couple stress, on (a) the couple stress and (b) the linear velocity fields, for shear in the absence of gravity. The curves are for four values of $m(0)$ in the allowed range $0 < m(0) < b$; the solid line is for $m(0) = b$. The velocity profiles for all the cases are indistinguishable. Here $\delta = 10°$, $\delta_L > \delta$, and other parameters are given in the caption of figure 2.

the boundary condition for $m(0)$ is largely unimportant in determining the velocity fields.

5.2. *Shear in a gravitational field*

Let us first consider the case where both walls have the same roughness, so that $\delta_L = \delta$. Equations (3.13) and (3.14) imply

$$\bar{\sigma}_{yx} = \text{constant}, \quad \frac{\mathrm{d}\bar{\sigma}_{yy}}{\mathrm{d}\xi} = -Bv. \tag{5.10}$$

Hence the ratio $|\bar{\sigma}_{yx}|/\bar{\sigma}_{yy}$ decreases with distance from the upper wall, and (4.2) cannot be satisfied at the lower wall if it holds at the upper wall. Therefore, for the reasons given in § 5.1 (for the case $\delta < \delta_L$), the boundary conditions are (4.1), (4.2) and (4.6) at the upper wall ($\xi = 1$), and (4.4) and (4.9) at the lower wall ($\xi = 0$).

As the normal stress $\bar{\sigma}_{yy}$ increases with distance from the upper wall, (3.5) implies that the solids fraction v also increases. However, in the regime of high solids fraction, a moderate change in σ_c causes only a small change in v. As gravitational compaction alone is usually sufficient to bring the solids fraction to a level close to maximum packing, we treat the material as incompressible, and the mean stress at critical state σ_c as an independent field. This approximation is used only to simplify the analysis; the variation in the body force can be easily be accounted for.

Figure 6 shows results for shear between fully rough walls under gravity, for four values of the parameter B. The solution for $B = 0$ corresponds to the uniform shear solution in the absence of gravity. As B increases, the velocity profile becomes curved, and shear is localized in a thin layer adjacent to the upper wall for large B. While the couple stress increases with distance from the upper wall, other Cosserat effects, such as the difference between ω and half the vorticity and the asymmetry in the Cauchy stress are maximum at the upper wall.

For large Couette gap, the asymptotic analysis in § A.2 provides an approximate solution. If the walls are not fully rough, the leading-order solution for the velocity fields is identical to that for gravity-free shear, given by (5.9) with $u_0 = 0$. If the walls are fully rough, there is a boundary layer of thickness $\sim \varepsilon^{2/3}$ near the upper wall within which m deviates from m_0. Consequently, the shear layer is thinner than in the zero gravity case (see § 8). The leading-order asymptotic solution for the couple stress

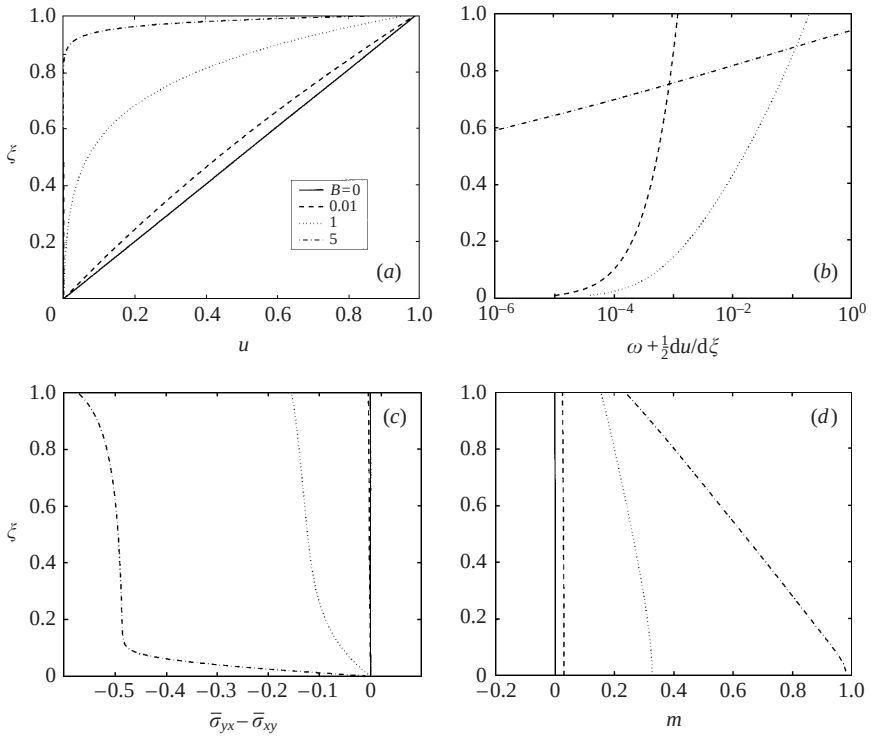

FIGURE 6. Predictions of the model for plane shear between fully rough walls under gravity; (*b*) shows the difference between ω and half the vorticity, and (*c*) shows the asymmetry in the shear stress. The solid line is absent in (*b*) because $\omega + (1/2)\,\mathrm{d}u/\mathrm{d}\xi = 0$ for this case. The parameter $B \equiv (\rho_p g H)/N$ indicates the strength of the gravitational body force. Other parameters are as in the caption of figure 2.

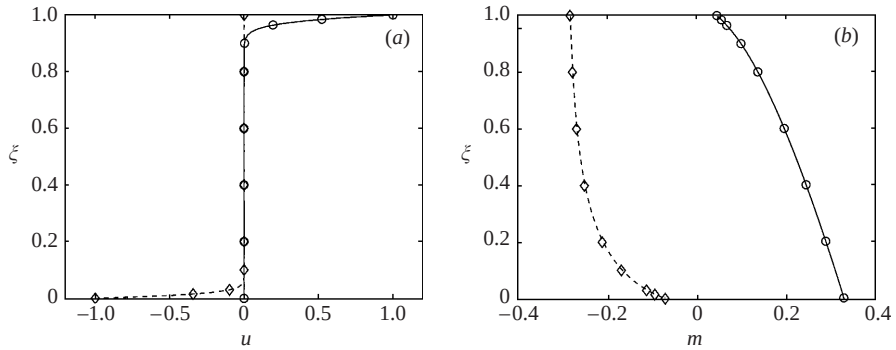

FIGURE 7. The asymptotic solutions for small ε compared with the numerical solutions for plane shear under gravity (circle and solid line respectively), and cylindrical Couette flow (diamond and dashed line respectively). The walls are fully rough for both cases. Parameter values are: $\phi = 28.5°$, $\varepsilon = 10^{-3}$, $L = 10$, $A = 1/3$, and $K = 0.5$. In addition, $B = 1$ for plane shear and $\bar{R}_i = 1$ for cylindrical Couette flow (see §6).

and velocity fields are compared with the numerical solution in figure 7, showing good agreement. As a small value of ε has been used, the slip velocity at the upper wall is negligible.

If δ_L is sufficiently smaller than δ, the friction boundary condition (4.2) can be satisfied at the lower wall. Assuming that the density of the material remains

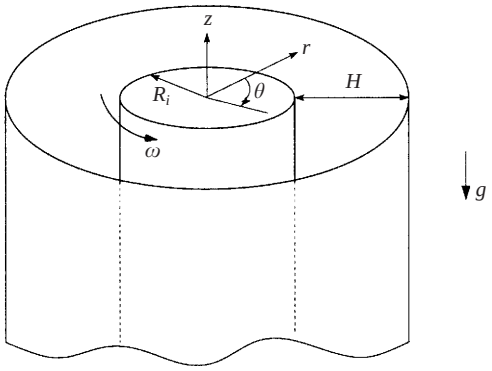

FIGURE 8. Schematic figure of cylindrical Couette flow. The outer cylinder is stationary and the inner cylinder rotates at constant angular velocity ω.

constant across the layer (see above), it is seen that (4.2) holds at the lower wall if $\tan\delta_L \leqslant \tan\delta/(1+Bv)$, and at the upper wall if $\tan\delta_L \geqslant \tan\delta/(1+Bv)$. The shear layer is adjacent to the lower wall in the former case, and adjacent to the upper wall in the latter (as in figure 6).

6. Cylindrical Couette flow

The cylindrical Couette cell is a common device for making rheological measurements. The material is confined between two vertical coaxial cylinders of radii R_i and $R_i + H$. Typically, the inner cylinder is rotated at constant speed, while the outer cylinder is kept stationary.

Using the cylindrical coordinates indicated in figure 8, the velocity field for steady axisymmetric flow is assumed to be of the form

$$v_r = 0, \quad v_z = 0, \quad v_\theta = v_\theta(r). \tag{6.1}$$

The only non-vanishing component of the vorticity is in the z-direction, and we expect the same for the intrinsic angular velocity,

$$\omega_r = \omega_\theta = 0, \quad \omega_z = \omega_z(r). \tag{6.2}$$

As in the case of plane shear (see § 3), the diagonal components of (2.8) imply equality of normal stresses,

$$\sigma_{rr} = \sigma_{\theta\theta} = \sigma_{zz} = \sigma_c. \tag{6.3}$$

It also follows from the flow rule (2.8) that all shear stresses except $\sigma_{r\theta}$ and $\sigma_{\theta r}$ vanish, and all couple stresses except M_{rz} vanish.

We note as an interesting aside that, as $\sigma_{rz} = 0$, there is no shear stress in the vertical direction on the walls of the Couette cell, regardless of either the wall roughness or the height of the material in the cell. In contrast, it is well known that the shear stress at the walls supports a part of the weight of a *static* granular column, leading to the so-called Janssen saturation of the stress with distance from the upper surface (Janssen 1895; Nedderman 1992, p. 84). While clear evidence as to whether or not this feature is preserved during flow is lacking, the data of Tardos *et al.* (1998) appear to be inconsistent with the Janssen solution. Nevertheless, measurements of σ_{rz} in cylindrical Couette flow have not been reported in the literature, and such measurements would provide a valuable check on the model predictions.

We introduce the dimensionless variables

$$\left.\begin{aligned} u &= \frac{v_\theta}{V_i}, \qquad \omega = \frac{\omega_z H}{V_i}, \quad \xi = \frac{r - R_i}{H}, \qquad \zeta = \frac{z}{H}, \\ \bar{\sigma}_{ij} &= \frac{\sigma_{ij}}{\rho_p g H}, \quad \bar{\sigma}_c = \frac{\sigma_c}{\rho_p g H}, \quad m = \frac{1}{L\sqrt{2(A+1)}} \frac{M_{rz}}{\rho_p\, g H d_p}, \end{aligned}\right\} \tag{6.4}$$

where R_i and V_i are the radius and the velocity of the inner cylinder, respectively. The yield condition (2.4*a*) then reduces to

$$(\bar{\sigma}_{r\theta}^2 + \bar{\sigma}_{\theta r}^2) + 2A\bar{\sigma}_{\theta r}\bar{\sigma}_{r\theta} + 4(A+1)^2 m^2 = 2(A+1)(\bar{\sigma}_c \sin\phi)^2. \tag{6.5}$$

As in § 3, the remaining components of the flow rule, after elimination of the factor $\dot{\lambda}/\tau$, yield

$$\frac{\mathrm{d}u}{\mathrm{d}\xi} - \frac{u}{(\bar{R}_i + \xi)} = -\left(\omega + \frac{u}{(\bar{R}_i + \xi)}\right) \frac{(A+1)(\bar{\sigma}_{\theta r} + \bar{\sigma}_{r\theta})}{(\bar{\sigma}_{\theta r} + A\bar{\sigma}_{r\theta})}, \tag{6.6}$$

$$\varepsilon\alpha \frac{\mathrm{d}\omega}{\mathrm{d}\xi} = -\left(\omega + \frac{u}{(\bar{R}_i + \xi)}\right) \frac{2(A+1)m}{(\bar{\sigma}_{\theta r} + A\bar{\sigma}_{r\theta})}, \tag{6.7}$$

which determine the variation of the velocity fields u and ω. Here, $\bar{R}_i \equiv R_i/H$, and $\varepsilon \equiv d_p/H$ is the ratio of the particle diameter to the Couette gap. An important point to note is that we must seek a solution in which the couple stress is negative, so the magnitude of ω (and the vorticity) decreases with distance from the inner cylinder, as is physically reasonable.

The mass balance is identically satisfied, and the balances of linear and angular momentum assume the form

$$\frac{\partial \bar{\sigma}_c}{\partial \xi} = \frac{C v u^2}{(1 + \xi/\bar{R}_i)}, \tag{6.8}$$

$$\frac{\partial \bar{\sigma}_{r\theta}}{\partial \xi} + \frac{\bar{\sigma}_{r\theta} + \bar{\sigma}_{\theta r}}{(\bar{R}_i + \xi)} = 0, \tag{6.9}$$

$$\frac{\partial \bar{\sigma}_c}{\partial \zeta} = -v, \tag{6.10}$$

$$\varepsilon\left(\frac{\partial m}{\partial \xi} + \frac{m}{(\bar{R}_i + \xi)}\right) = \bar{\sigma}_{r\theta} - \bar{\sigma}_{\theta r}, \tag{6.11}$$

where $C = V_i^2/(R_i g)$ is the Froude number. Note that (6.9) differs from the form given in most books on fluid mechanics, where the symmetry of the stress tensor is implicitly assumed.

We now show that the forms assumed for the velocity and angular velocity fields in (6.1)–(6.2) lead to an inconsistency. Equations (6.8) and (6.10) imply that $\bar{\sigma}_c = \bar{\sigma}_c(\xi, \zeta)$. Hence the yield condition (6.5) and the momentum balance (6.9) imply that $\bar{\sigma}_{r\theta}$, $\bar{\sigma}_{\theta r}$, and therefore the right-hand sides of (6.6) and (6.7), depend on ξ and ζ. However, their left-hand sides have been assumed to depend only on ξ. Thus it appears that we must relax some of the assumptions made above by allowing variation of u and ω with ζ, i.e. in the vertical direction, and also to allow a non-zero ω_r. This however leads to a large set of coupled partial differential equations whose solution appears to be a formidable task. This is contrary to our purpose of developing simple solutions that bring out the qualitative features of our model. However, it is possible construct a simple approximate solution, as described below.

We note that the above inconsistency arises because of the relation between the

shear and normal stresses through the yield condition. For a Newtonian fluid of constant viscosity, there is no such relation and hence no inconsistency in assuming a velocity field of the form given in (6.1).

For slow flows, the centripetal acceleration is small compared to the acceleration due to gravity, i.e. $C \ll 1$. We may therefore seek a solution as a regular perturbation in C, i.e. $m = m^{(0)} + Cm^{(1)} + C^2 m^{(2)} + \cdots$. For $C \ll 1$, the exact solution does not differ significantly from the leading-order solution of $O(C^0)$, except near the ends of the Couette cell where additional boundary conditions have to be satisfied. We therefore determine only the leading-order solution below, leaving the higher-order corrections to a later investigation.

At $O(C^0)$, it follows from (6.8) that $\bar{\sigma}_c$ is not a function of the radial position ξ, and hence $\bar{\sigma}_c = -v\zeta$ (the normal stress vanishes at the upper free surface). When this is substituted in the equations (6.6) and (6.7) to determine the velocity fields, there is no longer an inconsistency, and hence the simple forms of the velocity fields assumed in (6.1)–(6.2) are valid; in other words, when scaled by the hydrostatic head, the stress is independent of ζ. We now replace the definitions of the dimensionless stress and couple stress in (6.4) by the following:

$$\bar{\sigma}_{ij} = \frac{\sigma_{ij}}{\rho_p g H \bar{\sigma}_c}, \quad m = \frac{M_{rz}}{\rho_p g H \bar{\sigma}_c d_p L \sqrt{2(A+1)}}. \tag{6.12}$$

Equations (6.9) and (6.10) remain unchanged even after the above definitions. We note that our analysis is not applicable at the free surface, where the stresses vanish.

Consider the case where both walls have the same roughness. Referring to figure 8, $\bar{\sigma}_{r\theta} < 0$ at the inner cylinder ($\xi = 0$). If it is assumed that $\bar{\sigma}_{\theta r}$ has the same sign as $\bar{\sigma}_{r\theta}$, (6.9) implies that $\bar{\sigma}_{r\theta}$ decreases in magnitude as ξ increases. (Our results are consistent with this assumption.) As (6.8) and (6.12) imply that $\bar{\sigma}_{rr}$ is a constant, the ratio $|\bar{\sigma}_{r\theta}|/\bar{\sigma}_{rr}$ decreases with distance from the inner cylinder. Therefore, the friction boundary condition applies at the inner cylinder, but cannot be satisfied at the outer cylinder. This situation is identical to that at the lower wall for the case of plane shear under gravity. We therefore follow the arguments outlined in § 5.2 and adopt boundary conditions

$$\bar{\sigma}_{r\theta} = \bar{\sigma}_{\theta r}, \quad u = 0 \tag{6.13}$$

at the outer cylinder ($\xi = 1$). At the inner cylinder ($\xi = 0$), we use the friction and slip boundary conditions

$$\bar{\sigma}_{r\theta} = -\tan\delta, \quad u = -1 - \varepsilon K \omega, \tag{6.14a,b}$$

where we have the inner cylinder rotating in the anti-clockwise direction (see figure 8). In the limit $\bar{R}_i \to \infty$, (6.14*a*) holds at the outer cylinder also. Hence the velocity boundary condition $u = \varepsilon K \omega$ is applied at the outer wall. This corresponds to plane shear between walls of equal roughness in the absence of gravity, discussed in § 5.1.

The governing equations (6.5)–(6.11), with boundary conditions (6.13)–(6.14), are integrated using the procedure described in § 5.1. The stress and velocity profiles for the case of fully rough walls are presented in figure 9 for four values of $\bar{R}_i$. As expected, we recover the uniformly shearing solution for plane shear in the limit $\bar{R}_i \to \infty$. The localization of shear near the inner cylinder increases as $\bar{R}_i$ decreases. Though the magnitude of the couple stress is maximum at the outer cylinder, the asymmetry of the Cauchy stress and the deviation of ω from half the vorticity are maximum at the inner cylinder.

The solution for large Couette gap is provided by the asymptotic analysis in § A.3.

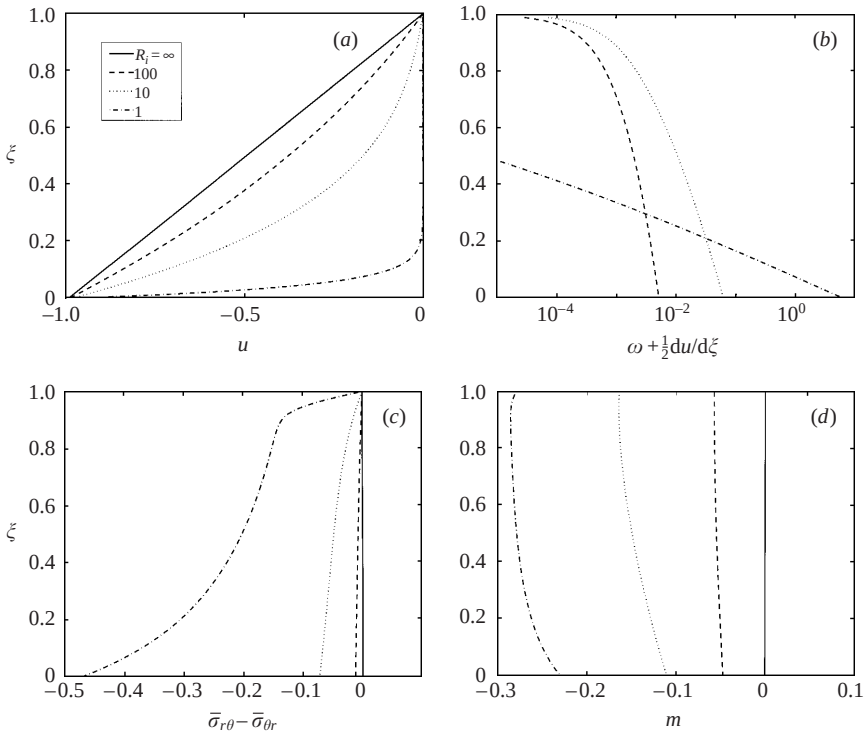

FIGURE 9. Profiles of the stress and kinematic fields for shear between fully rough walls in a cylindrical Couette cell for four values of $\bar{R}_i$, the ratio of the inner cylinder radius to the Couette gap; (*b*) shows the difference between ω and half the vorticity, and (*c*) shows the asymmetry in the shear stress. The solid line is absent in (*b*) because $\omega + (1/2)\,\mathrm{d}u/\mathrm{d}\xi = 0$ for this case. $\bar{R}_i = \infty$ (solid line) corresponds to plane shear, for which ω is equal to the vorticity and the Cauchy stress is symmetric. Parameter values are: $\phi = 28.5°$, $\varepsilon = 0.04$, $L = 10$, $A = 1/3$ and $K = 0.5$.

The leading-order solution is the same as in plane shear (with or without gravity) when the walls are not fully rough. If the walls are fully rough, the solution is similar in form to that for plane shear under gravity: the couple stress rises to m_0 within a boundary layer of thickness $\sim \varepsilon^{2/3}$ near the inner cylinder, and remains at m_0 outside the boundary layer. The velocity fields are determined by the couple stress within the boundary layer, and are independent of the wall roughness. The leading-order asymptotic solution for the velocity fields is compared with the numerical solution for fully rough walls in figure 7.

6.1. *Comparison with experimental data*

Experimental measurements of the velocity profile in cylindrical Couette flow of granular materials have recently been reported by Mueth *et al.* (2000) and Losert *et al.* (2000). Mueth *et al.* (2000) used mustard and poppy seeds and obtained the velocity profiles using magnetic resonance imaging. Losert *et al.* (2000) used glass beads and measured the velocity profile by video imaging of the upper surface of the granular column; they also applied upward aeration across the granular column, and observed that it has negligible effect on the velocity profile. From the data reported in their papers, we have determined the parameter $\mathscr{R}$, defined in § 1, to be in the range 6×10^{-9}–10^{-3} for the experiments of Mueth *et al.* (2000), and 7×10^{-9}–2×10^{-4} for those of Losert *et al.* (2000). The Froude number C, defined below (6.11), for the two

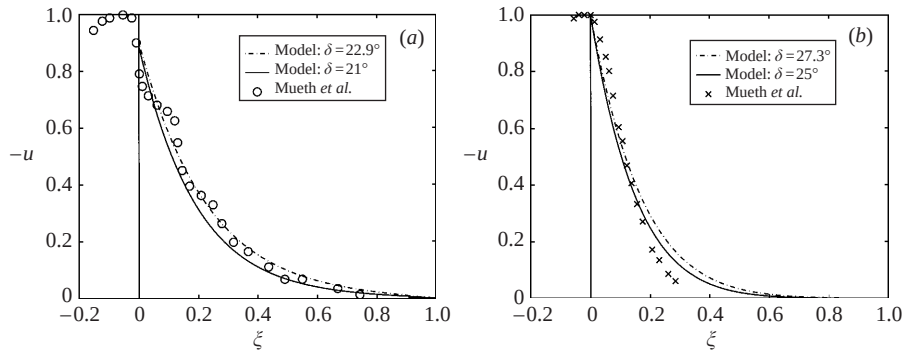

FIGURE 10. Comparison of model predictions (curves) with the data (symbols) of Mueth *et al.* (2000) for shear of (*a*) mustard seeds and (*b*) poppy seeds in a cylindrical Couette cell. In the experiments, a layer of particles was glued to the cylinders. The data points to the left of $\xi = 0$ are the velocity of the glued layer. The dot-dash line represents the model prediction for fully rough walls ($\tan\delta = \sin\phi$, see (4.3)). See text for other parameters.

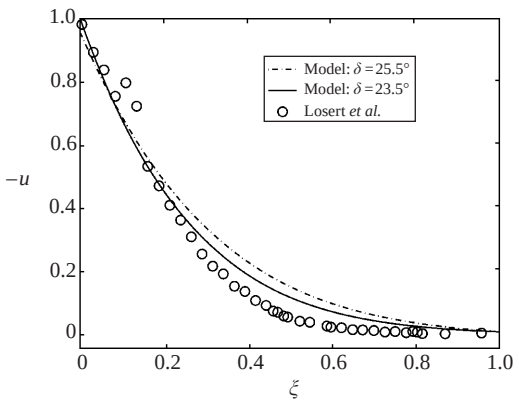

FIGURE 11. Comparison of model predictions (curves) with the data (symbols) of Losert *et al.* (2000) for the shear of glass beads in a cylindrical Couette cell. In the experiments, a layer of particles was glued to the cylinders. The dot-dash line represents the model prediction for fully rough walls ($\tan\delta = \sin\phi$, see (4.3)). See text for other parameters.

studies was in the range 10^{-6}–6×10^{-2} and 2×10^{-6}–2×10^{-2}, respectively. As $\mathscr{R}$ and C are both small for these studies, it is appropriate to compare our model predictions with their data. Both find that the shape of the velocity profile is independent of the rotation rate of the inner cylinder, which, of course, is also a feature of our model.

The predictions of the velocity profile using our Cosserat model are compared with the data of Mueth *et al.* (2000) in figure 10 and with the data of Losert *et al.* (2000) in figure 11. In both studies, the inner and outer cylinders were coated with a layer of particles; we have therefore taken the walls to be at the outer edges of the glued layers for the purpose of comparison. Neither of the studies has reported the angle of internal friction of the material they used. For mustard seeds, Tüzün & Nedderman (1985) report it to be in the range 23°–25°, and we have used $\phi = 25°$ for our calculations. Data on this property are lacking for the more angular and rough poppy seeds, and we have taken the value of 31°. For glass beads, we have used the value of $\phi = 28.5°$ reported by Nott (1991). The value of K was set by matching the wall slip velocity to the reported values, yielding $K = 0.65$ for mustard seeds, and

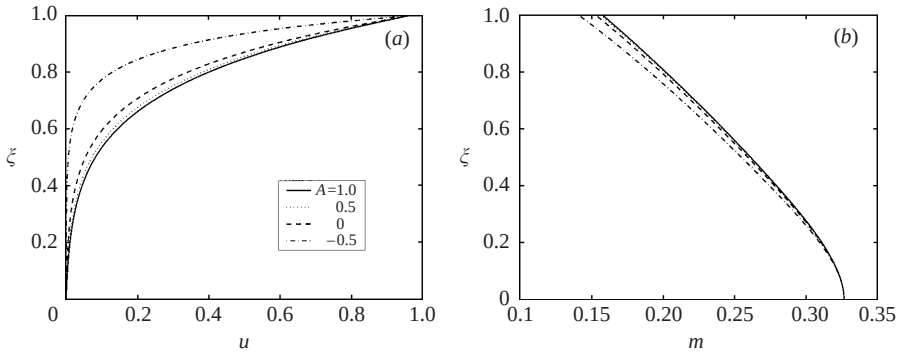

FIGURE 12. Sensitivity of model predictions to the parameter A in the yield condition (3.16). The solutions are for plane shear between fully rough walls under gravity with $B = 1$. As discussed in § 2.1, $|A|$ must be $\leqslant 1$, and for the set of parameters used here, solutions do not exist for $A < -0.57$. The values of other parameters are as in the caption of figure 2.

zero for poppy seeds and glass beads. No attempt was made to determine the best-fit values of L and A, and the values used so far in the paper have been retained, namely $L = 10$, $A = 1/3$. The values of ε and R_i, determined from reported values of the mean grain diameter and the dimensions of the Couette cell are $\varepsilon = 0.15$, 0.058 and 0.067, and $\bar{R}_i = 2.29$, 1.89 and 4.25 for mustard, poppy and glass, respectively.

The dot-dash lines in figures 10 and 11 are model predictions assuming fully rough walls ($\tan\delta = \sin\phi$), and the solid lines are predictions for δ roughly 2° lower than $\tan^{-1}(\sin\phi)$. We find that the latter fits the data better, in agreement with our argument in § 5.1 that a fully rough wall may be difficult to achieve practically. It is clear that there is, in general, good agreement between the model predictions and the data. Though our model overestimates the velocity for glass beads (figure 11), we must bear in mind that we have only made plausible guesses for almost all the material properties, and have not attempted to achieve a better fit by adjusting the parameters.

Our model predicts only a small increase in the solids fraction with distance from the inner cylinder (if the assumption of incompressibility is relaxed), while the data of Mueth *et al.* (2000) suggest a substantial variation. In spite of this difference, the predicted velocity profiles are in good agreement with their data. Thus it appears that the velocity field is relatively insensitive to the dilation of the granular medium.

7. Parameter sensitivity of model predictions

The properties of the material and the boundaries in the Cosserat model are characterized by the angles of internal friction ϕ, the angles of wall friction δ_L and δ, the parameters $A \equiv a_2/a_1$ and L occurring in the yield condition (2.4*b*), and the parameter K that determines the extent of slip at a boundary in the boundary condition (4.5). The significance of the angles of friction is well understood; their physical meaning remains the same as in classical plasticity models. We now consider the sensitivity of the model to the parameters A and K, which are associated with Cosserat effects in our model. To this end, we consider the problem of plane shear under gravity, and explore the effect of varying these parameters.

As discussed in § 2.1, A can assume values only in the range $(-1, 1)$. However, solutions may not exist for all negative values of A within this range, as illustrated in figure 12. For the set of values of the other parameters used here, the shear stress σ_{xy}

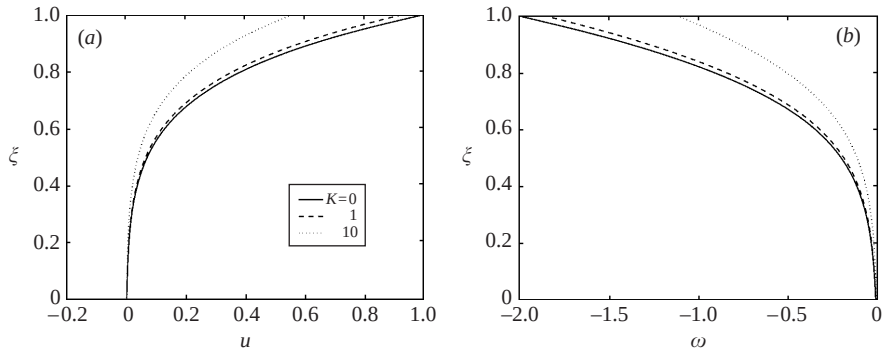

FIGURE 13. Sensitivity of model predictions to the parameter K in the kinematic boundary condition (4.5). The solutions are for shear between fully rough walls under gravity with $B = 1$. As K increases, the slip velocity at the upper wall increases and the magnitude of the angular velocity at the wall decreases. The stress and couple stress profiles are not affected by the value of K, and are given by the dotted lines in figure 6. The values of parameters other than K are as in the caption of figure 2.

assumes complex values when $A < -0.57$, and hence a physically acceptable solution does not exist. Solutions exist for $-0.57 < A < 1$, and figure 12 shows that in this range of values, there is not much variation in the velocity profile and even less in the couple stress.

The parameter K determines the extent of velocity slip at the boundaries, but does not affect the stress and couple stress fields. As shown in figure 13, there is no slip at the upper wall when $K = 0$, and the velocity slip increases with K. The important point is that the shapes of the velocity profiles are unaltered by varying K, a result which is also shown clearly by the asymptotic solutions in the Appendix.

8. Shear layer thickness

Though our model assumes that the granular material yields everywhere within the Couette gap, the results in the preceding two sections show the velocity decaying rapidly with distance from the upper wall for plane shear (with the exception of gravity-free shear between fully rough walls), and from the inner cylinder for cylindrical Couette flow. In the experiments of Mueth *et al.* (2000) and Losert *et al.* (2000), grain motion is not detectable beyond a distance of a few particle diameters from the wall. It is therefore useful to define the dimensionless shear layer thickness Δ as the distance, in terms of particle diameters, from the upper wall (or the inner cylinder) at which the velocity decays to a small fraction f of the wall velocity,

$$(u(1 - \varepsilon\Delta) - u_0) = f(u(1) - u_0) \quad \text{for plane shear,} \tag{8.1a}$$

$$(u(\varepsilon\Delta) - u_0) = f(u(0) - u_0) \quad \text{for cylindrical Couette flow.} \tag{8.1b}$$

The reference velocity u_0 is equal to zero, except in the case of gravity-free plane shear between identical walls, where it is $1/2$ (the velocity at the centre). We set $f = 0.05$, as in earlier studies, and determine the shear layer thickness as a function of the Couette gap, or equivalently, ε. While Δ must in general be determined numerically, an analytical expression can be obtained in the limit of large Couette gap ($\varepsilon \to 0$), as discussed below.

In most practical instances of granular flow, the size of the vessel is much larger than the grain size. It is therefore useful to determine the dependence of the shear layer thickness Δ on the system size in the limit $\varepsilon \to 0$. In our earlier work on flow

in vertical channels (Mohan *et al.* 1999), we showed that in the limit of small ε, Δ is independent of ε, except in the singular case of a fully rough wall ($\tan\delta = \sin\phi$), when it grows as $\epsilon^{-1/3}$. Here, we apply the same approach to determine the asymptotic behaviour of Δ for plane and cylindrical Couette flow.

For each of the problems considered, the leading-order asymptotic solutions for the stress and velocity fields are given in the Appendix. These suffice to determine the shear layer thickness. The details of the asymptotic analysis are given in the Appendix, and the solutions are used here to determine the shear layer thickness.

When the walls are not fully rough, i.e. $\tan\delta < \sin\phi$, the leading-order linear velocity fields for plane shear and cylindrical Couette flow may be written in the common form (5.9*d*) (see (A 3*b*) and (A 4*b*)), where the reference velocity u_0 is as defined below (8.1). The shear layer thickness can now be determined using (5.9*d*) and (8.1),

$$\Delta = -\ln(f)/k = \frac{2.996L\tan\delta}{2(\sin^2\phi - \tan^2\delta)^{1/2}}. \tag{8.2}$$

Thus, we find Δ to be independent of the Couette gap when the latter is large compared to particle size (i.e. $\varepsilon \ll 1$). A feature observed in some experiments is that the shear layer thickness decreases as the wall becomes smoother (Nedderman & Laohakul 1980), and this too is captured by (8.2).

We note that the shear layer thickness increases as $\tan\delta$ approaches $\sin\phi$. In the precise limit of fully rough walls, the solution was given in § 5.1 for plane shear in the absence of gravity, showing that shear rate is equal throughout the gap, and therefore $\Delta = (1-u_0)(1-f)\varepsilon^{-1}$. Thus, the parameter L does not determine the thickness of the shear layer when the walls are fully rough, in contrast to the case of non-fully rough walls. In the former case, the couple stress vanishes, and hence the governing equations do not involve L.

For shear under gravity and cylindrical Couette flow, the material does not shear uniformly for fully rough walls, and the asymptotic velocity profile (5.9*d*) is not valid in a region of thickness $\sim\varepsilon^{2/3}$ near the upper wall and inner cylinder, respectively. A uniformly valid solution is found by rescaling ξ and m in this 'inner' region, as shown in § A.2 and § A.3, and the leading-order velocity profile then assumes the form

$$u = 1 - I(\hat{\xi})/I(\infty). \tag{8.3}$$

where

$$I(\hat{\xi}) \equiv (\mathrm{Ai}(0))^{-2}\int_0^{\hat{\xi}} (\mathrm{Ai}(z))^2\,\mathrm{d}z.$$

Here $\mathrm{Ai}(x)$ is the Airy function, and the rescaled independent variable is

$$\hat{\xi} = \begin{cases} (1-\xi)\varepsilon^{-2/3}\left(\dfrac{L^2}{2Bv}\right)^{-1/3} & \text{for plane shear under gravity,} \\ \xi\varepsilon^{-2/3}\left(\dfrac{L^2\bar{R}_i}{4}\right)^{-1/3} & \text{for cylindrical Couette flow.} \end{cases} \tag{8.4}$$

The value of $\hat{\xi}$ at which (8.1) holds is found to be 1.275, resulting in the following

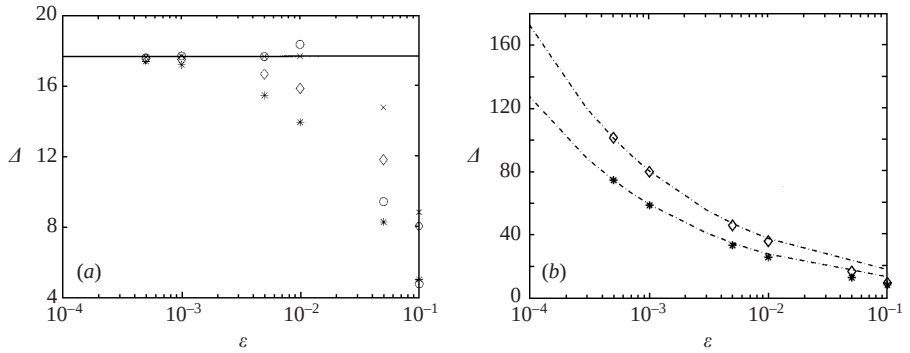

FIGURE 14. The shear layer thickness Δ as a function of ε for plane shear and cylindrical Couette flow: (*a*) for a non-fully rough upper wall (or inner cylinder), and (*b*) for fully rough walls. In both panels, the curves represent asymptotic solutions for small ε, given in § 8, and the symbols represent numerical solutions. The circles and crosses are for plane shear in the absence of gravity between identical (but not fully rough) walls and with a rougher lower wall, respectively; the asterisks are for plane shear under gravity and the diamonds are for cylindrical Couette flow. Parameter values for (*a*) are: $\phi = 28.5°$, $\delta = 20°$, $L = 10$, $A = 1/3$ and $K = 0.5$, $B = 1$ (for plane shear under gravity) and $\bar{R}_i = 1$ (for cylindrical Couette flow); (*b*) the same except that $\delta = \tan^{-1}\sin\phi = 25.5°$.

expression for the shear layer thickness:

$$\Delta = \begin{cases} 1.275\varepsilon^{-1/3}\left(\dfrac{L^2}{2Bv}\right)^{1/3} & \text{for plane shear under gravity,} \\ 1.275\varepsilon^{-1/3}\left(\dfrac{L^2\bar{R}_i}{4}\right)^{1/3} & \text{for cylindrical Couette flow.} \end{cases} \tag{8.5}$$

Thus, Δ grows as the one-third power of the ratio of the Couette gap to grain size when the walls are fully rough. In contrast, Δ is independent of the Couette gap (cf. (8.2)) when the walls are not fully rough. It also grows as $(Bv)^{-1/3}$, in plane shear under gravity, as the gravitational body force is reduced, but the above asymptotic analysis is not valid when $Bv \sim \varepsilon$. In the limit $B = 0$, which corresponds to plane shear without gravity, the solution in § 5.1 shows a linear velocity profile, and therefore $\Delta = (1-u_0)(1-f)\varepsilon^{-1}$. Similarly Δ grows as $(\bar{R}_i)^{1/3}$, in cylindrical Couette flow, as the radius of the inner cylinder increases, and approaches $(1-u_0)(1-f)\varepsilon^{-1}$ in the limit $\bar{R}_i \to \infty$.

The variation of Δ with ε is shown in figure 14 for plane and cylindrical Couette flow; panel (*a*) shows the results for non-fully rough walls and panel (*b*) for fully rough walls. The symbols are the numerical results obtained by the procedure described in §§ 5 and 6, and the lines are the asymptotic solutions. For non-fully rough walls, the shear layer thickness for all the four problems converges to the common asymptote of $\Delta \approx 17.67$ as $\varepsilon \to 0$, as shown in figure 14(*a*). For shear between fully rough walls, the numerical solutions for Δ asymptote to the forms given by (8.5) as $\varepsilon \to 0$.

9. Other models

Models for the shear of dense granular materials have also been proposed recently by Savage (1998) and Losert *et al.* (2000). Here we briefly discuss some aspects of their models.

9.1. *The model of Savage (1998)*

In a recent paper, Savage (1998) proposed a model that attempts to merge the critical state theory for quasi-static flows with the results from kinetic theory for rapid flows, with the stated primary aim of predicting the behaviour of transitional and rapid flows. The model starts with a yield condition and an associated flow rule (as in this work), but Savage argues that the rate of deformation tensor $\boldsymbol{D}$ at any location fluctuates in time, with a standard deviation ϵ. The mean stress tensor $\langle \boldsymbol{\sigma} \rangle$ is determined by computing its average with respect to a Gaussian distribution of deformation rates. In the limit $|\langle D_{ij} \rangle| \ll \epsilon$, where D_{ij} is a component of $\boldsymbol{D}$, a Newtonian constitutive relation is obtained for $\langle \boldsymbol{\sigma} \rangle$, with the shear viscosity given by $\sigma_c A/\epsilon$, where σ_c is the frictional mean stress at a critical state and A is a material constant. In order to obtain a theory which resembles kinetic theories for rapid flow, it is assumed that σ_c may be replaced by $\sigma_{c1}(\nu) + \sigma_{c2}(\nu, T)$. Here σ_{c1} is the frictional mean stress, σ_{c2} is the mean stress obtained from kinetic theory, and T is the grain temperature or equivalently, the kinetic energy of velocity fluctuations. To proceed further, it is assumed that ϵ is proportional to $\sqrt{T}$, and the proportionality constant is determined by matching the form obtained for large values of T with the corresponding kinetic theory result.

The idea of accounting for fluctuations in the deformation rate appears to have merit, but we find the following aspects of the model unconvincing. (i) The physical origin of large fluctuations in the velocity gradients relative to the mean velocity gradients is not clear. Data bearing on this issue do not appear to be available in the literature. (ii) Even though the constitutive relations are derived by assuming that $|\langle D_{ij} \rangle| \ll \epsilon$, this ratio turns out to be $O(1)$ in the examples discussed in Savage (1998). Thus the theory is applied beyond its range of validity. As noted by Savage (1998), some of the kinetic constitutive equations also suffer from this defect when applied to plane shear. (iii) As the velocity gradients are decomposed into mean values and fluctuations, it appears that the inertial terms, which involve products of velocity fluctuations, may contribute non-zero terms to the averaged momentum balances. Such terms have been omitted in the analysis. (iv) The solution of bounded flow problems requires the specification of the grain temperature at the boundaries, which is usually unknown *a priori*; realistically one would like to determine the temperature as part of the solution.

9.2. *The model of Losert et al. (2000)*

This is a minor variant of the high-density kinetic theory of Haff (1983), though Losert *et al.* (2000) have arrived at the high-density limit using the kinetic theory of Jenkins & Savage (1983). The only change the authors have made is in proposing a modified expression for the shear viscosity; this gives a better fit for their data of the grain temperature as a function of the shear rate. Making some simplifying assumptions about the form of the temperature profile, they determine the velocity profile with three adjustable parameters. It is shown that the profile provides a good fit to their data for shear in a cylindrical Couette cell (see figure 11). However, their solution is derived for plane shear, whereas the data they compare with (and achieve a good fit) are for cylindrical Couette flow.

More importantly, it seems likely that the underlying assumptions of kinetic theory, such as molecular chaos and instantaneous binary collisions, will break down in the limit of small deformation rate and high solids fraction. Therefore, as in the case of Savage's model discussed above, it appears that the theory has been used beyond its range of validity. Even if one were to just view the high-density kinetic theory as a

phenomenological model, its applicability to slow granular flow is suspect as it does not yield a rate-independent stress for small deformation rates.

10. Summary and conclusions

We have shown that our frictional Cosserat model for slow granular flows captures the formation of thin shear layers in viscometric flows. The principal features of our continuum model are: (i) the presence of a couple stress field, which is a result of tangential frictional forces between grains; (ii) an angular velocity field which is not necessarily determined by the local vorticity; (iii) solution of the balance of angular momentum, in addition to the balances of mass and linear momentum; (iv) the extension of the yield condition and flow rule used in classical plasticity to incorporate the couple stress and the angular velocity. By including these features, we incorporate a microscopic length scale in our model, which determines the thickness of the shear layer.

For plane shear in the absence of gravity, we have considered two cases: in the first, the two walls are of equal roughness, and in the second, the upper wall is smoother. In the first, for which the shear rate is symmetric about the mid-plane, we find that Cosserat effects (a finite couple stress, asymmetry of the Cauchy stress tensor and deviation of the angular velocity from half the vorticity) are maximum near the solid boundaries, and decay with distance from the boundaries. In the second case, the couple stress is finite everywhere in the gap, but other Cosserat effects are absent. In both cases, the velocity fields decay rapidly with distance from the upper wall if the Couette gap is large compared to the grain size. If the roughness of the granular medium is exactly equal to that of the wall, it shears uniformly in the entire gap.

For shear between walls of equal roughness in a gravitational field (and in cylindrical Couette flow), the couple stress is finite throughout the Couette gap, but other Cosserat effects are present only in the shear layer near the upper wall (inner cylinder). Here too the velocity and angular velocities decay rapidly with distance from the upper wall (inner cylinder). While experimental measurements of the couple stress or asymmetry in the Cauchy stress have not been reported, our predictions are in good agreement with the velocity measurements reported recently by Mueth *et al.* (2000) and Losert *et al.* (2000).

If the wall roughness is less than that of the granular medium (i.e. $\tan\delta < \sin\phi$), the shear layer thickness Δ increases with the Couette gap, but reaches an asymptotic value independent of the Couette gap in the limit $H/d_p \to \infty$ (H and d_p are the Couette gap and grain diameter, respectively). Further, Δ decreases when the angle of wall friction δ is reduced, and vanishes when the wall is perfectly smooth, in qualitative agreement with available experimental data. In the singular case of fully rough walls ($\tan\delta = \sin\phi$), the material shears uniformly over the entire Couette gap for plane shear in the absence of gravity; for plane shear under gravity or cylindrical Couette flow, Δ increases with the Couette gap as $(H/d_p)^{1/3}$, and does not depend on ϕ.

Many of the above predictions regarding the behaviour of Δ have so far not been confirmed experimentally. We believe that these are important issues to be probed in future experimental investigations, as they will serve to distinguish between existing models for slow granular flows. Another prediction we make, also requiring experimental verification, is that the shear layer is located near the lower wall (outer cylinder) if it is sufficiently smoother than the upper wall (inner cylinder), and the material elsewhere suffers little deformation.

While the predictions of our model are for the particular forms of the constitutive relations (namely the yield condition and the flow rule) and the boundary conditions we have chosen, we believe that the main qualitative features of our results have a general validity. For instance, the yield condition (2.4*a*) is a modification of the extended von Mises yield condition, a relation between the first and second invariants of $\boldsymbol{\sigma}$; by incorporating the couple stress in this relation, we introduce a microscopic length scale naturally into the constitutive relations. Any other yield condition, such as that proposed by Lade & Duncan (1975) (extended to allow critical states) which involves also the third invariant, could also be modified in the same spirit, and the qualitative effect would be the same: the microscopic length scale will set the length scale for the thickness of the shear layer.

In cylindrical Couette flow, our model predicts a small increase in the solids fraction (depending on the magnitude of the Froude number C) as we move towards the outer cylinder. This increase, however, is substantially smaller than what was observed in the experiments of Mueth *et al.* (2000). This defect may perhaps be corrected by incorporating elastic effects in the model, which is a direction worthy of further study. For example, Tejchman & Gudehus (2001) have found that the use of a Cosserat model based on hypoplasticity permits the density to vary across the shear layer. Nevertheless, we believe that our model is a natural extension of classical plasticity models for slow granular flows.

While the models of Losert *et al.* (2000) and Savage (1998) also attempt to explain thin shear layers, they do not yield a rate-independent stress, which has shown to be an important characteristic of slow flows. In any case, further experiments are required to assess the performance of our model and others in various flow problems, before attempting to decide which model, if any, is more realistic.

Appendix A. Asymptotic solution for small ε

To determine the asymptotic behaviour for small ε, we seek a perturbation solution of the form

$$m = m^{(0)} + \varepsilon m^{(1)} + \varepsilon^2 m^{(2)} + \cdots \tag{A 1}$$

for the couple stress, and similarly for the other fields. For each of the problems considered, we derive only the leading-order solutions of $O(\varepsilon^0)$ for the stress and velocity fields, as they suffice to determine the shear layer thickness. However, we ensure that the asymptotic expansion is uniformly valid by checking that the ratio $m^{(1)}/m^{(0)}$ is $O(1)$ everywhere in the domain $0 < \xi < 1$.

A.1. *Plane shear in the absence of gravity*

On substituting (A 1) in (5.3), we find that the leading-order solution for the stresses is

$$\bar{\sigma}^{(0)}_{xy} = \bar{\sigma}_{yx} = -\tan\delta, \tag{A 2a}$$

$$m^{(0)} = m_0 \equiv \sqrt{b^2 - a^2}, \tag{A 2b}$$

and the solutions at all higher orders in ε vanish. The constants a and b are defined in (5.4). This asymptotic solution is valid only in the outer region $\xi - 1/2 \gg \varepsilon$; in the inner region $(\xi - 1/2) \sim \varepsilon$, m deviates from m_0 to satisfy (5.1*a*), as evident from the exact solution (5.5). For fully rough walls, $m_0 = 0$, and hence (A 2) is a uniformly valid solution as it satisfies the boundary condition $m(1/2) = 0$.

The ω and u fields in the outer region are obtained from (3.17)–(3.18) and (A 2), yielding

$$\omega = \frac{-1/2}{\varepsilon(K + 2/k)} \exp(-k(1-\xi)/\varepsilon), \tag{A 3a}$$

$$u = \frac{1}{2}\left(1 + \frac{2/k}{(K + 2/k)} \exp(-k(1-\xi)/\varepsilon)\right), \tag{A 3b}$$

where k is defined in (5.8*d*). Thus, the linear and angular velocities decay rapidly with distance from the walls. The variation of m within the inner region near $\xi = 1/2$ has little influence on the velocity and fields, as they are negligibly small within this region.

When the two walls are of different roughness, the exact solution is given in § 5.1. The couple stress is constant, $m = m_0$, regardless of ε, and the solutions for ω and u given in (5.8*b*) reduce in the asymptotic limit to

$$\omega = \frac{-1}{\varepsilon(K + 2/k)} \exp(-k(1-\xi)/\varepsilon), \tag{A 4a}$$

$$u = \frac{2/k}{(K + 2/k)} \exp(-k(1-\xi)/\varepsilon). \tag{A 4b}$$

It should be noted that if the couple stress at the lower wall is changed by replacing (4.4) with an alternative boundary condition (see § 4), the asymptotic solution for m in the outer region $\xi \gg \varepsilon$ will still be $m = m_0$, but the solution in the inner region $\xi \sim \varepsilon$ will be different. However, the velocity fields are affected only by the couple stress in the outer region, as they decay rapidly with distance from the upper wall, and therefore the boundary condition for m at $\xi = 0$ does not influence the velocity profile in the limit $\varepsilon \to 0$.

A.2. *Plane shear under gravity*

An equation for the couple stress, similar to (5.3) for zero gravity, can be obtained by combining the yield condition and the angular momentum balance, to give

$$\alpha\varepsilon \frac{\mathrm{d}m}{\mathrm{d}\xi} = -a + (b^2 + c^2[(1 + Bv(1-\xi))^2 - 1] - m^2)^{1/2}, \tag{A 5}$$

where $c^2 = \sin^2\phi/(2A + 2)$, and a and b are defined in (5.4).

Substituting (A 1) in (A 5), the solution at the first two orders in ε is

$$m^{(0)} = (m_0^2 + c^2[(1 + Bv(1-\xi))^2 - 1])^{1/2}, \tag{A 6a}$$

$$m^{(1)} = \frac{ac^2\alpha}{{m^{(0)}}^2}[B^2v^2(1-\xi) + Bv], \tag{A 6b}$$

with m_0 defined in (A 2*b*). Unlike in § A.1, the expression for $m^{(0)}$ above is valid in the entire domain $0 < \xi < 1$, as it satisfies the boundary condition (4.4) at the lower wall. To determine if the expansion is uniformly valid, we inspect the ratio $\varepsilon m^{(1)}/m^{(0)}$. When $\tan\delta < \sin\phi$, the ratio is $O(\varepsilon)$. Thus the above asymptotic expansion is uniformly valid when the walls are not fully rough. The leading-order solutions for the velocity and angular velocity, obtained by integrating (3.17) and (3.18), are

$$\omega^{(0)} = \omega_1 \exp\left(-\frac{k}{\varepsilon}\int_\xi^1 \left(1 + \left(\frac{c}{m_0}\right)^2 [(1 + Bv(1-\xi'))^2 - 1]\right)^{1/2} \mathrm{d}\xi'\right), \tag{A 7a}$$

$$u^{(0)} = -2\int_0^{\xi} \omega(\xi')\,\mathrm{d}\xi', \tag{A 7b}$$

where $\omega_1 = \omega(1)$ and k is defined in (5.8d). To simplify the above expressions, we anticipate the rapid decay of the velocity within a region of thickness $O(\varepsilon)$ from the upper wall, substitute $\bar{\xi} = (1-\xi)/\varepsilon$ and expand in ε. Retaining only the leading-order terms for consistency, we obtain expressions for the velocity fields which are identical to (A 4), the latter corresponding to shear in the absence of gravity.

For the singular case of fully rough walls ($\tan\delta = \sin\phi$), $m^{(0)}(1) = 0$. Hence the asymptotic expansion (A 6) is not valid in a region near the upper wall where $(1-\xi) \sim \varepsilon^{2/3}$, because the ratio $\varepsilon m^{(1)}/m^{(0)}$ is $O(1)$ within this region. Noting that the scaling for the latter is exactly what we obtained for flow through a vertical channel (Mohan *et al.* 1999), we follow the same procedure to determine a uniformly valid asymptotic expansion in the entire domain $0 < \xi < 1$.

To determine the solution within the inner region near the upper wall, we follow the prescription of Van Dyke (1964, pp. 20 and 569) and introduce the following rescaled variables:

$$\hat{\xi} = (1-\xi)\varepsilon^{-2/3}\left(\frac{L^2}{2Bv}\right)^{-1/3}, \quad \hat{m} = m\varepsilon^{-1/3}(4a\alpha Bvc^2)^{-1/3}, \tag{A 8}$$

and seek a solution a solution of the form $\hat{m} = \hat{m}^{(0)} + f(\varepsilon)\hat{m}^{(1)} + \cdots$. Upon substituting the above in (A 5), we get at leading order

$$-\frac{\mathrm{d}\hat{m}^{(0)}}{\mathrm{d}\hat{\xi}} + (\hat{m}^{(0)})^2 - \hat{\xi} = 0. \tag{A 9}$$

This is a Riccati equation, whose solution can be written in terms of the Airy functions (Bender & Orszag 1984, pp. 20, 569),

$$\hat{m}^{(0)} = -\frac{\mathrm{d}}{\mathrm{d}\hat{\xi}}\ln(c_1\mathrm{Ai}(\hat{\xi}) + c_2\mathrm{Bi}(\hat{\xi})). \tag{A 10}$$

where $\mathrm{Ai}(\hat{\xi})$ and $\mathrm{Bi}(\hat{\xi})$ are the two independent Airy functions and c_1 and c_2 are constants of integration. The constants are determined by matching the inner and outer solutions in an overlap region, as suggested by Van Dyke (1964, p. 105). Upon writing the outer solution (A 6a) in terms of the inner variable $\hat{\xi}$ and expanding for small ε, we determine the leading-order term to be $(4a\alpha Bvc^2)^{1/3}\varepsilon^{1/3}\hat{\xi}^{1/2}$. This must match with the leading-order outer expansion of the inner solution, which is

$$-(4a\alpha Bvc^2)^{1/3}\varepsilon^{1/3}\hat{\xi}^{1/2} \quad \text{if} \quad c_1 = 0, \quad (4a\alpha Bvc^2)^{1/3}\varepsilon^{1/3}\hat{\xi}^{1/2} \quad \text{if } c_2 = 0. \tag{A 11}$$

Hence $c_2 = 0$ and the solution at leading order in the inner region is

$$m^{(0)} = -\varepsilon^{1/3}\frac{(4a\alpha Bvc^2)^{1/3}}{\mathrm{Ai}(\hat{\xi})}\frac{\mathrm{d}}{\mathrm{d}\hat{\xi}}(\mathrm{Ai}(\hat{\xi})), \tag{A 12}$$

from which we may derive the uniformly valid (additive) composite solution in the entire domain,

$$m^{(0)} = c([1+Bv(1-\xi)]^2-1)^{1/2} - \varepsilon^{1/3}\frac{(4a\alpha Bvc^2)^{1/3}}{\mathrm{Ai}(\hat{\xi})}\frac{\mathrm{d}}{\mathrm{d}\hat{\xi}}(\mathrm{Ai}(\hat{\xi})) - (2Bvc^2(1-\xi))^{1/2}. \tag{A 13}$$

In the same manner, the uniformly valid solutions for the velocity fields at the leading

order are found to be

$$\omega = \omega_1 \left(\frac{\mathrm{Ai}(\hat{\xi})}{\mathrm{Ai}(0)} \right)^2, \quad u - u_1 = \varepsilon^{2/3} \left(\frac{L^2}{2Bv} \right)^{1/3} 2\omega_1 I(\hat{\xi}), \tag{A 14a, b}$$

where $\omega_1 = \omega(1)$, $u_1 = u(1)$ and

$$I(\hat{\xi}) \equiv (\mathrm{Ai}(0))^{-2} \int_0^{\hat{\xi}} (\mathrm{Ai}(z))^2 \mathrm{d}z. \tag{A 15}$$

Enforcing the boundary condition $u(0) = 0$ and the velocity boundary condition (4.6) at the upper wall, the angular velocity and velocity at the wall can be determined, giving to leading order

$$\omega_1 = \frac{-\varepsilon^{-2/3}}{2} \left(\frac{L^2}{2Bv} \right)^{-1/3} \frac{1}{I(\infty)}, \quad u_1 = 1. \tag{A 16a, b}$$

The uniformly valid velocity profile to leading order therefore is

$$u = 1 - I(\hat{\xi})/I(\infty). \tag{A 17}$$

A.3. *Cylindrical Couette flow*

Subtracting (6.11) from (6.9) and integrating, we obtain the following relation between the shear stress $\bar{\sigma}_{r\theta}$ and the couple stress:

$$\bar{\sigma}_{r\theta} = \frac{-\tan\delta}{(1 + \xi/\bar{R}_i)^2} + 2(A+1)\varepsilon\alpha \left(\frac{m}{(\bar{R}_i + \xi)} - \frac{m(0)\bar{R}_i}{(\bar{R}_i + \xi)^2} \right). \tag{A 18}$$

At $O(\varepsilon^0)$, (6.11) and (A 18) result in $\bar{\sigma}_{\theta r} = \bar{\sigma}_{r\theta} = -\tan\delta/(1 + \xi/\bar{R}_i)^2$, which when substituted in the yield condition (6.5) gives the leading-order couple stress,

$$m^{(0)} = -\left(m_0^2 + d^2 \left[1 - \frac{1}{(1 + \xi/\bar{R}_i)^4} \right] \right)^{1/2} \tag{A 19}$$

where $d^2 = \tan^2\delta/2(A+1)$. At $O(\varepsilon)$, (6.5) and (6.11), together with (A 18), yield

$$m^{(1)} = \frac{a\alpha}{(m^{(0)})^2 \bar{R}_i (1 + \xi/\bar{R}_i)^3} \left(m_0^2 + d^2 \left[1 - \frac{3}{(1 + \xi/\bar{R}_i)^4} \right] \right) - \frac{2a\alpha m^{(0)}(0)}{m^{(0)} \bar{R}_i (1 + \xi/\bar{R}_i)^4}. \tag{A 20}$$

Here too $\varepsilon m^{(1)}/m^{(0)} \sim O(\varepsilon)$, except when $\tan\delta = \sin\phi$. Therefore the above expansion is uniformly valid when the wall is not fully rough. On integrating (6.6)–(6.7) and expanding the results for the region $\xi \sim \varepsilon$ near the inner cylinder, we see that the leading-order velocity fields are again identical to (A 4).

As in § A.2, the above asymptotic expansion for m is not uniformly valid when the inner cylinder is fully rough, as the ratio $\varepsilon m^{(1)}/m^{(0)}$ is $O(1)$ in the inner region $\xi \sim \varepsilon^{2/3}$. A solution in the inner region may be found by re-scaling the variables,

$$\hat{\xi} = \xi \varepsilon^{-2/3} \left(\frac{L^2 \bar{R}_i}{4} \right)^{-1/3}, \quad \hat{m} = \frac{m}{d} \varepsilon^{-1/3} \left(\frac{4L}{\bar{R}_i} \right)^{-1/3}, \tag{A 21}$$

yielding the following equation for $\hat{m}^{(0)}$:

$$\frac{\mathrm{d}\hat{m}^{(0)}}{\mathrm{d}\hat{\xi}} + (\hat{m}^{(0)})^2 - \hat{\xi} = 0. \tag{A 22}$$

Following the procedure given in § A.2, the uniformly valid expression for the couple stress is

$$m^{(0)} = -d\left(1 - \frac{1}{(1+\xi/\bar{R}_i)^4}\right)^{1/2} + \varepsilon^{1/3}\frac{d(4L/\bar{R}_i)^{1/3}}{\mathrm{Ai}(\hat{\xi})}\frac{\mathrm{d}}{\mathrm{d}\hat{\xi}}(\mathrm{Ai}(\hat{\xi})) + d(4\xi/\bar{R}_i)^{1/2}, \quad (\mathrm{A}\,23)$$

and for velocity fields is

$$\omega = \frac{-\varepsilon^{-2/3}}{2}\left(\frac{L^2\bar{R}_i}{4}\right)^{-1/3}\frac{1}{I(\infty)}\left(\frac{\mathrm{Ai}(\hat{\xi})}{\mathrm{Ai}(0)}\right)^2, \quad (\mathrm{A}\,24a)$$

$$u = -1 + I(\hat{\xi})/I(\infty), \quad (\mathrm{A}\,24b)$$

where $I(\hat{\xi})$ is defined by (A 15).

REFERENCES

Albert, R., Pfeifer, M. A., Barabasi, A. & Schiffer, P. 1999 Slow drag in a granular medium. *Phys. Rev. Lett.* **82**, 205–208.

Albert, R., Tegzes, P., Kahng, B., Albert, L., Sample, J., Pfeifer, M., Barabasi, A., Vicsek, T. & Schiffer, P. 2000 Jamming and fluctuations in granular drag. *Phys. Rev. Lett.* **84**, 5122–5125.

Bender, C. M. & Orszag, S. A. 1984 *Advanced Mathematical Methods for Scientists and Engineers.* McGraw Hill.

Besdo, D. 1974 Ein beitrag zur nichtlinearen theorie des Cosserat-kontinuums. *Acta Mech.* **20**, 105–131.

de Borst, R. 1993 A generalisation of the J_2-flow theory for polar continua. *Comput. Meth. Appl. Mech. Engng* **103**, 347–362.

Brennen, C. & Pearce, J. C. 1978 Granular material flow in two dimensional hoppers. *Trans. ASME: J. Appl. Mech.* **45**, 43–50.

Budny, T. J. 1979 Stick-slip friction as a method of powder flow characterization. *Powder Technol.* **23**, 197–201.

Campbell, C. S. 1993 Boundary interaction for two-dimensional granular flows. Part 1. Flat boundaries, asymmetric stresses and couple stresses. *J. Fluid Mech.* **247**, 111–136.

Cleaver, J. A. S. & Nedderman, R. M. 1993 Theoretical prediction of stress and velocity profiles in conical hoppers. *Chem. Engng Sci.* **48**, 3693–3702.

Dahler, J. S. 1959 Transport phenomena in a fluid composed of diatomic molecules. *J. Chem. Phys* **30**, 1447–1475.

Gudehus, G. & Tejchman, J. 1991 Some mechanisms of a granular mass in a silo-model tests and a numerical Cosserat approach. In *Advances in Continuum Mechanics* (ed. O. Brüller, V. Mannel & J. Najar), pp. 178–194. Springer.

Haff, P. K. 1983 Grain flow as a fluid-mechanical phenomenon. *J. Fluid Mech.* **134**, 401–430.

Howell, D., Behringer, R. P. & Veje, C. 1999 Stress fluctuations in a 2d granular couette experiment: a continuous transition. *Phys. Rev. Lett.* **82**, 5241–5244.

Jackson, R. 1983 Some mathematical and physical aspects of continuum models for the motion of the granular materials. In *Theory of Dispersed Multiphase Flow* (ed. R. E. Meyer), pp. 291–337. Academic.

Janssen, H. A. 1895 Versuche uber getriededruck in silozellen (on the measurement of pressures in grain silos). *Z. Ver. Deut. Ing.* **39**, 1045–1049.

Jaunzemis, W. 1967 *Continuum Mechanics.* Macmillan.

Jenkins, J. T., Cundall, P. A. & Ishibashi, I. 1989 Micromechanical modeling of granular materials with the assistance of experiments and numerical simulations. In *Powders and Grains* (ed. Biarez & Gourvès), pp. 257–264. A. A. Balkema.

Jenkins, J. T. & Savage, S. B. 1983 A theory for the rapid flow of identical, smooth, nearly elastic, spherical particles. *J. Fluid Mech.* **130**, 187–202.

Kaza, K. R. 1982 The mechanics of flowing granular materials. PhD thesis, University of Houston.

Lade, P. V. & Duncan, J. M. 1975 Elastoplastic stress-strain theory for cohesionless soil. *J. Geotech. Engng Div. ASCE* **101**, 1037–1053.

Lippmann, H. 1995 Cosserat plasticity and plastic spin. *Appl. Mech. Rev.* **48**, 753–762.

Losert, W., Bocquet, L., Lubensky, T. C. & Gollub, J. P. 2000 Particle dynamics in sheared granular matter. *Phys. Rev. Lett.* **85**, 1428–1431.

Michalowski, R. L. 1987 Flow of granular media through a plane parallel/converging bunker. *Chem. Engng Sci.* **42**, 2587–2596.

Mohan, L. S., Nott, P. R. & Rao, K. K. 1997 Fully developed flow of coarse granular materials through a vertical channel. *Chem. Engng Sci.* **52**, 913–933.

Mohan, L. S., Nott, P. R. & Rao, K. K. 1999 A frictional cosserat model for the flow of granular materials through a vertical channel. *Acta Mech.* **138**, 75–96.

Mueth, D. M., Detregeas, G. F., Karczmar, G. S., Eng, P. J., Nagel, S. R. & Jaeger, H. M. 2000 Signatures of granular microstructure in dense shear flows. *Nature* **406**, 385–389.

Mühlhaus, H. B. 1986 Shear band analysis in granular materials by Cosserat theory. *Ing. Archiv.* **56**, 389–399.

Mühlhaus, H. B. 1989 Application of cosserat theory in numerical solution of limit load problems. *Ing. Arch.* **59**, 124–137.

Mühlhaus, H. B. & Vardoulakis, I. 1987 The thickness of shear bands in granular materials. *Géotechnique* **37**, 271–283.

Munch-Andersen, J. & Askegaard, V. 1993 Silo model tests with sand – and grain. In *Proc. Intl Symp. on Reliable Flow of Particulate Solids II*. Norway.

Nasuno, S., Kudrolli, A., Bak, A. & Gollub, J. 1998 Time-resolved studies of stick-slip friction in sheared granular layers. *Phys. Rev.* E **58**, 2161–2171.

Natarajan, V. V. R., Hunt, M. L. & Taylor, E. D. 1995 Local measurements of velocity fluctuations and diffusion coefficients for a granular material flow. *J. Fluid Mech.* **304**, 1–25.

Nedderman, R. M. 1992 *Statics and Kinematics of Granular Materials.* Cambridge University Press.

Nedderman, R. M. & Laohakul, C. 1980 The thickness of shear zone of flowing granular materials. *Powder Technol.* **25**, 91–100.

Nott, P. R. 1991 Analysis of granular flow in aerated and vibrated chuetes. PhD thesis, Princeton University.

Petzold, L. 1983 Automatic selection of methods for solving stiff and nonstiff systems of ordinary differential equations. *SIAM J. Sci. Statist. Comput.* **4**, 136–148.

Savage, S. B. 1998 Analyses of slow high-concentration flows of granular materials. *J. Fluid Mech.* **377**, 1–26.

Schofield, A. N. & Wroth, C. P. 1968 *Critical State Soil Mechanics.* McGraw-Hill.

Tardos, G. I., Khan, M. I. & Schaeffer, D. G. 1998 Forces on a slowly rotating, rough cylinder in a couette device containing a dry, frictional powder. *Phys. Fluids* **10**, 335–341.

Tejchman, J. & Gudehus, G. 1993 Silo-music and silo-quake experiments and a numerical Cosserat approach. *Powder Technol.* **76**, 201–212.

Tejchman, J. & Gudehus, G. 2001 Shearing of a narrow granular layer with polar quantitites. *Intl J. Numer. Anal. Meth. Geomech.* **25**, 1–28.

Tejchman, J. & Wu, W. 1993 Numerical study of patterning of shear bands in a Cosserat continuum. *Acta Mech.* **99**, 61–74.

Tejchman, J. & Wu, W. 1994 Numerical study on sand and steel interfaces. *Mech. Res. Commun.* **21** (2), 109–119.

Tüzün, U. & Nedderman, R. M. 1985 Gravity flow of granular materials round obstacles—II. *Chem. Engng Sci.* **40**, 337–351.

Van Dyke, M. 1964 *Perturbation Methods in Fluid Mechanics.* Academic.